The Levantine Basin—crustal structure and origin

G.L. Netzeband [a,*], K. Gohl [b,1], C.P. Hübscher [a,2], Z. Ben-Avraham [c,3],
G.A. Dehghani [a,4], D. Gajewski [a,5], P. Liersch [a,6]

[a] Institut für Geophysik, Universität Hamburg, Bundesstraße 55, 20146 Hamburg, Germany
[b] Alfred-Wegener-Institute for Polar and Marine Research, Am Alten Hafen 26, 27568 Bremerhaven, Germany
[c] Tel Aviv University, Department of Geophysics and Planetary Sciences, P.O.B. 39040, Ramat Aviv, Tel Aviv, 69978, Israel

Abstract

The origin of the Levantine Basin in the Southeastern Mediterranean Sea is related to the opening of the Neo-Tethys. The nature of its crust has been debated for decades. Therefore, we conducted a geophysical experiment in the Levantine Basin. We recorded two refraction seismic lines with 19 and 20 ocean bottom hydrophones, respectively, and developed velocity models. Additional seismic reflection data yield structural information about the upper layers in the first few kilometers. The crystalline basement in the Levantine Basin consists of two layers with a P-wave velocity of 6.0–6.4 km/s in the upper and 6.5–6.9 km/s in the lower crust. Towards the center of the basin, the Moho depth decreases from 27 to 22 km. Local variations of the velocity gradient can be attributed to previously postulated shear zones like the Pelusium Line, the Damietta–Latakia Line and the Baltim–Hecateus Line. Both layers of the crystalline crust are continuous and no indication for a transition from continental to oceanic crust is observed. These results are confirmed by gravity data. Comparison with other seismic refraction studies in prolongation of our profiles under Israel and Jordan and in the Mediterranean Sea near Greece and Sardinia reveal similarities between the crust in the Levantine Basin and thinned continental crust, which is found in that region. The presence of thinned continental crust under the Levantine Basin is therefore suggested. A β-factor of 2.3–3 is estimated. Based on these findings, we conclude that sea-floor spreading in the Eastern Mediterranean Sea only occurred north of the Eratosthenes Seamount, and the oceanic crust was later subducted at the Cyprus Arc.

* Corresponding author. Tel.: +49 40 42838 5045; fax: +49 40 42838 5441.
  E-mail addresses: netzeband@dkrz.de (G.L. Netzeband), kgohl@awi-bremerhaven.de (K. Gohl), huebscher@dkrz.de (C.P. Hübscher),
zvi@terra.tau.ac.il (Z. Ben-Avraham), ali@dkrz.de (G.A. Dehghani), gajewski@dkrz.de (D. Gajewski), liersch@dkrz.de (P. Liersch).
[1] Tel.: +49 471 4831 1361; fax: +49 471 4831 1271.
[2] Tel.: +49 40 42838 5184; fax: +49 40 42838 5441.
[3] Tel.: +972 3 6408528; fax: +972 3 6409282.
[4] Tel.: +49 40 42838 2978; fax: +49 40 42838 5441.
[5] Tel.: +49 40 42838 2975; fax: +49 40 42838 5441.
[6] Tel.: +49 40 42838 5045; fax: +49 40 42838 5441.

1. Introduction

The early evolution of the Levantine Basin in the Southeastern Mediterranean Sea is closely related to the history of the Neo-Tethys. Determining whether the crust in the basin is continental or oceanic is crucial for reconstruction of the Neo-Tethys opening and the position of its spreading axes. Whereas the continental character of the crust under the Eratosthenes Seamount and Cyprus is undisputed (Makris et al., 1983; Hirsch,

1984; Garfunkel, 1998; Robertson, 1998a), the nature of the crust underlying the Levantine Basin is still a matter of debate. Many authors, e.g., Ginzburg and Ben-Avraham (1987) and Ben-Avraham et al. (2002) postulate old oceanic crust under the basin, with the age varying from Triassic (Freund et al., 1975) to Cretaceous (Dercourt et al., 1986). According to these theories, the Eratosthenes Seamount was separated from the African margin in the Permian (Garfunkel, 1998) along with other continental fragments (Ben-Avraham
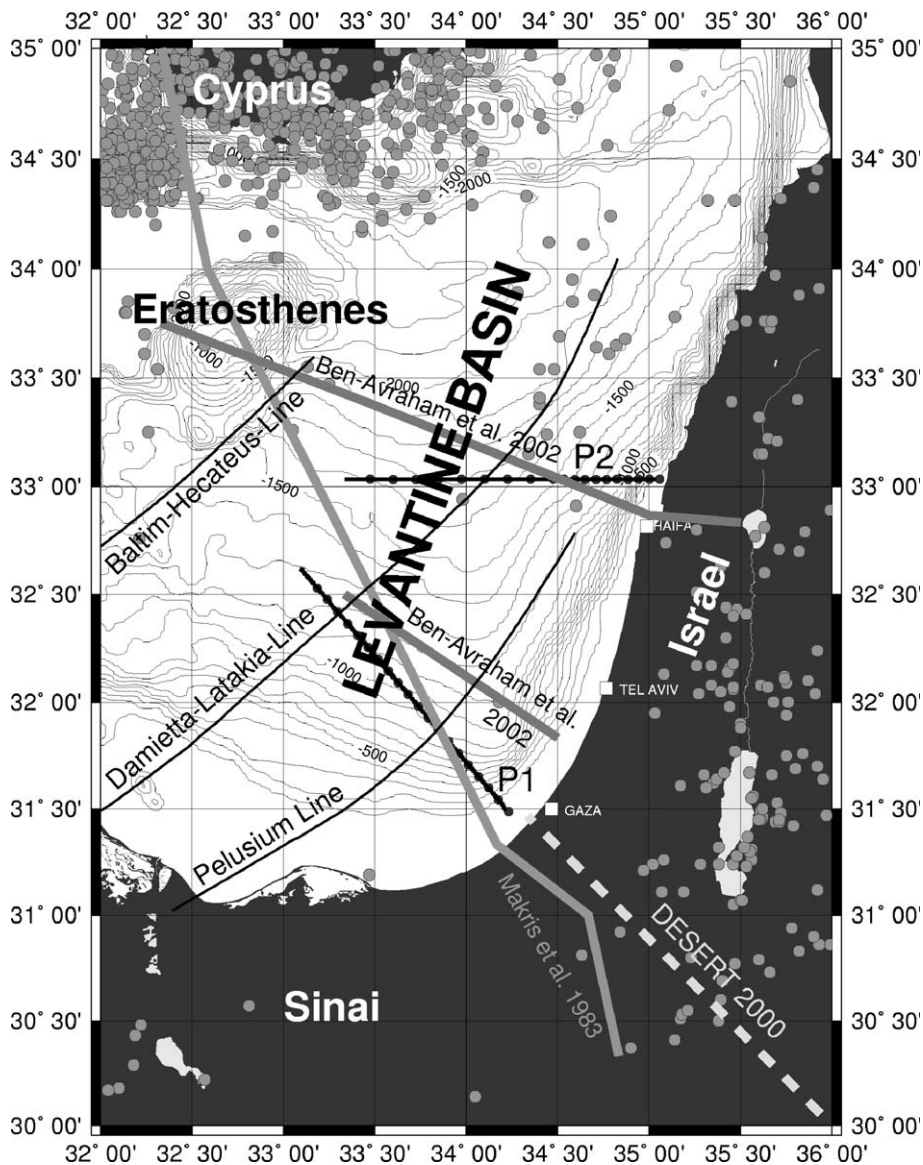

Fig. 1. Map of the Levantine Basin. Thick solid lines mark the locations of profiles P1 and P2, with solid black circles indicating the positions of the OBH. The shear zones Pelusium Line, Damietta–Latakia Line, and Baltim–Hecateus Line are shown after Neev et al. (1976). Gray circles mark hypocenters of earthquakes since 1973 according to the US Geological Survey. Previous refraction seismic lines in the Levantine Basin are marked as light gray lines.

and Ginzburg, 1990) and migrated northwards, where it presently collides with Cyprus (Robertson, 1998b) with an annual collision rate of approximately 1 cm/year (Kempler and Garfunkel, 1994; Albarello et al., 1995). Other authors claim that the crust under the Levantine Basin is continental (Woodside, 1977; Hirsch, 1984; Hirsch et al., 1995; Vidal et al., 2000a) and argue that it was part of the Triassic African–Arabian plate system (Hirsch, 1984).

Several plate tectonic reconstructions have been developed, differing in aspects as the origin of the crust under the Levantine Basin, the age of this crust, the location of the spreading axes and how far the Neo-Tethys was opened before subduction set in (Hirsch et al., 1995; Garfunkel, 1998; Robertson, 1998a,b; Stampfli and Borel, 2002). Hirsch et al. (1995) draws the Triassic Neo-Tethys with a width in N–S direction of approximately 700 km north of Arabia and shows the African–Arabian margin including the area of the present Levantine Basin covered by a shallow sea. In the Jurassic, according to this study, the Tethys reaches a width of 2400 km and is in the Late Cretaceous reduced to approximately 200 km in the area of the present Mediterranean Sea. Garfunkel (1998) postulates rifting between Israel and the Eratosthenes Seamount as early as in the Permian. In the Late Triassic, two rifting axes are described by Garfunkel (1998), one east and one west of the Eratosthenes, and a spreading axis north of the seamount, perpendicular to the rifting. Robertson (1998a,b) dates the rifting phase that separated the Eratosthenes from the Levant margin to the Late Triassic, assuming oceanic crust in the Levantine Basin only north of 32°30′N (present-day coordinates). Stampfli and Borel (2002) show an elaborate global-scale plate reconstruction focussing on the Tethys area, giving a general idea on the Paleozoic and Mesozoic plate movements, but the Levantine Basin in particular is not resolved. Mascle et al. (2000) found evidence for a Levantine–Sinai continental microplate extending from the Red Sea to roughly 35°N including the Eratosthenes Seamount and bounded to the east by the Dead Sea Transform Fault and identified this microplate as a fragment of the African craton.

Two refraction seismic studies to analyse the crustal structure have been conducted previously in the Levantine Basin (Makris et al., 1983; Ben-Avraham et al., 2002) consisting of three profiles (Fig. 1). Further deep seismic studies have been carried out onshore by Ginzburg et al. (1979, 1994), El-Isa et al. (1987) and, recently, the DESERT2000 project (Weber et al., 2004), providing information on the crustal structure under Israel, Jordan and the Sinai Peninsula.

In 2002, a multidisciplinary cruise (the GEMME-Project, M52/2) was carried out with the R/V *Meteor* in order to unravel the nature and origin of the crust under the Levantine Basin. A grid of reflection seismic lines and two new refraction seismic lines with a close receiver spacing were recorded along with gravity measurements and echosounder (Parasound) data. The crustal structure along these refraction lines will be the topic of this study.

2. Geological and geophysical setting

The Eastern Mediterranean, and with, it the Levantine Basin, is a relic of the Mesozoic Neo-Tethys Ocean (Robertson and Dixon, 1984; Stampfli and Borel, 2002; Garfunkel, 2004). The Levantine Basin is confined by the Israeli and the Egyptian coasts, Cyprus and the Eratosthenes Seamount (Fig. 1). In the Miocene, the so-called 'Messinian Salinity Crisis' was initiated by the disconnection of the Mediterranean to the Atlantic. This was caused by a combination of tectonic uplift and sea level changes (Hsü et al., 1973, 1978) and led to a drop of sea level, a rise in salt concentration and finally to precipitation (e.g., Gradmann et al., 2005). The evaporite layer deposited during that time in the Levantine Basin is up to 2 km thick.

The basin has undergone significant subsidence for more than 100 Ma (Mart, 1982; Tibor et al., 1992; Almagor, 1993; Vidal et al., 2000a), over 2 km since Pliocene (Mart, 1982) and is still subsiding (Tibor et al., 1992). The basement is buried under up to 14 km of sediments (Ben-Avraham et al., 2002). The slope on the shelf steepens from 4° off Sinai to over 10° off northern Israel (Mart, 1984). Faults trending NE–SW have been observed onshore (Mart, 1982) and offshore (Neev et al., 1976; Abdel Aal et al., 2000; Farris et al., 2004). A fold belt, which extends from the Western Desert of Egypt through Sinai into the Palmyra folds of Syria has been termed the Syrian Arc (Walley, 1998). In its central segment, at the latitudes of Israel and Lebanon, it strikes NNE–SSW. The Pelusium Line (Fig. 1), a prominent fault line runs ca. 35–50 km offshore subparallel to the Israeli coastline (Neev, 1975, 1977; Neev et al., 1976; Mart, 1982; Hirsch et al., 1995). The Pelusium line represents the western edge of the Syrian Arc fold belt. The evolution of this regional compressional tectonic feature began in the Late Cretaceous and continued until the Early–Middle Miocene (Walley, 1998; Gardosh and Druckmann, in press). Its evolution was related to the closure of the Neo-Tethys (see Garfunkel, 1998, 2004 for comprehensive summaries).

3. Previous work

There has been a number of geophysical studies in the Levantine Basin. Three seismic refraction lines were recorded (Ben-Avraham et al., 2002) (Fig. 1), two in 1989 (Ben-Avraham et al., 2002) and one in 1979 (Makris et al., 1983; Ginzburg and Ben-Avraham, 1987). On these lines, about 10 receivers per line were used; therefore, receiver spacing was at least twice as wide as in our study.

The models of these refraction seismic lines show a Moho depth of 20–25 km. A single crustal layer of 6.7 km/s was observed and interpreted as oceanic crust. Two crustal layers were observed under Israel, with a P-wave velocity of 6.7 km/s in the lower crust and the velocity in the upper crust varying from 6.3 km/s under northern Israel to 6.0 km/s in the south. The pinch-out of the upper crust was located 20 km offshore on the northern profile and 100 km offshore on the southern line and interpreted as the transition zone between continental and oceanic crust. On all these lines, accompanying gravity and magnetic models were compiled, which based on the refraction seismic models and showed matching results. Deep seismic experiments analysing the crust under Israel, Negev and Jordan have been carried out by Ginzburg et al. (1979, 1994), El-Isa et al. (1987) and, recently, in the frame of the DESERT2000 project (Weber et al., 2004) (Fig. 1) and show a crustal thickness under Judea of less than 30 km, thinning to the north to slightly over 20 km under Galilee–Lebanon and thickening to the south and east to up to 40 km beneath Negev and Jordan. The mantle depth under the Eratosthenes Seamount has been modeled to 28 km. Analysis of the magnetic field of the Levantine Basin by Ben-Avraham and Ginzburg (1986) revealed no typical elongated alternating magnetic anomalies typical of oceanic crust. The authors, nevertheless, maintained their idea of oceanic crust and offered two explanations for the missing anomalies: (1) The crust could have been created in an era without polarity reversals. (2) The magnetic anomalies could have been destroyed by later crustal deformation. Woodside (1977) analysed the gravity and magnetic field of the Eastern Mediterranean Sea, but came to a different conclusion. He states that there is evidence for the northward continuation of crustal structure from northern Egypt into the Eastern Mediterranean Basin and concludes that the crust under the Levantine Basin represents the thinned margin of the African plate. Hirsch et al. (1995) and Vidal et al. (2000a,b) show reflection seismic lines which image the basin structure down to the basement. Both are located at the top of the basement at ca. 12 km on average and agree that the basement is not flat but faulted with displacements of up to 500 m. Based on the reflective character of the basement, the structure of the top basement unconformity and the large thickness of Mesozoic sediments, Vidal et al. (2000a) favour the hypothesis of strongly attenuated continental crust in the Levantine Basin.

Above the basement, the depositional sequences are identified as Cretaceous–Jurassic, Paleogene–Neogene, Messinian and Pliocene–Holocene (Vidal et al., 2000b; Abdel Aal et al., 2000). The Cretaceous–Jurassic unit above the basement has been interpreted as a carbonate sequence with a P-wave velocity of 4.5 km/s (Ben-Avraham et al., 2002). The layer above represents Post-Cretaceous to Pre-Messinian sediments with a velocity of 3.8–4.0 km/s (Vidal et al., 2000a), accumulated in 60 Ma during the subsidence of the basin. The Messinian sequence consists of Messinian evaporites, precipitated during the Messinian Salinity Crisis. This sequence comprises a high velocity of more than 4.0 km/s (Mart and Ben-Gai, 1982), and the reflections marking top and bottom of this layer have been termed M- and N-reflection, respectively (Ryan et al., 1970). On top of the Messinian evaporites, Nile sediments have been deposited since the re-flooding of the Mediterranean (Mart, 1982).

4. New geophysical data

The data of this study were collected during the cruise M52/2 with the German research vessel R/V *Meteor* in 2002 (Pätzold et al., 2003).

4.1. Seismic refraction data—acquisition

Two seismic refraction lines were acquired (Fig. 1). On line P1, the number of 20 ocean bottom hydrophones (OBH) were deployed over a distance of 150 km, line P2 consists of 19 OBH deployed along 158 km. In the prolongation of line P2, a seismic station was set up onshore (33°02.508′N/35°07.167′E). All of the instruments on line P2 recorded data, but on line P1, five OBHs (1, 2, 8, 12, and 19) failed and two more (6 and 14) showed only the direct wave, because of insufficient amplification. The sampling rate of the OBHs was 4 ms, that of the onshore station 5 ms. Two 32l-Bolt Airguns were used as the source with a shot spacing of 125 m (60 s).

4.2. Seismic refraction data—processing and characteristics

Prior to analysis, the seismic refraction data were re-positioned and processed with a band-pass filter passing

frequencies of 3–25 Hz. On some stations, signals were enhanced by application of a 1-s automatic gain control (AGC). Generally, data quality suffered from harsh weather conditions, the thick sedimentary layer in the Levantine Basin that absorbs a significant amount of seismic energy and also from the Messinian salt layer, where a great part of the seismic energy is refracted. Predictive deconvolution did not help much in signal enhancement (Fig. 2a), the appearance of the modified signals is slightly clearer, but the arrivals cannot be traced significantly farther than before the deconvolution. At greater offsets, where a wrap-around of the direct wave of the previous shot appeared, an F–K filter was applied in order to reduce the amplitudes of the wrap-around. Nevertheless, new arrivals were not revealed (Fig. 2b).

Fig. 3a–c shows the recordings of the station 07 in the center of line P1, and station 17 and 18 on line P2 on the shelf end. In the near offsets of Fig. 3a, steep reflections from the top of the evaporite layer (PeP) can be observed, but the first arrivals belong to turning waves within this layer (Pe). The Pe arrivals are very prominent throughout the line; they are observed on every station, as well as the PeP. Later arrivals in Fig. 3a are reflections from the top of the carbonate layer (PcarbP) which are observed on eight other stations as well, and the top of the upper crust (PcuP), which is also seen on a number of other recordings. A weak Moho reflection (PmP) appears at an offset of 40 km at 8 s. Five stations recorded PmP arrivals; a Pn phase consisting of waves turning within the upper mantle was detected on four stations. Internal crustal reflections, named PclP, were observed on only two stations, OBH 09 and OBH 17.

At OBH 17 on line P2 (Fig. 3b) PeP arrivals, and turning waves from both sediment blocks, Ps1 and Ps2, are observed. From an offset of 40 km, the refraction of the upper crust, Pcu, can be seen, and at 60 km, the refraction of the upper crust, Pcl, appears. At an offset of approximately 75 km, the Pn, turning waves of the upper mantle, arrive. At OBH 18 (Fig. 3c), the PeP and Pe
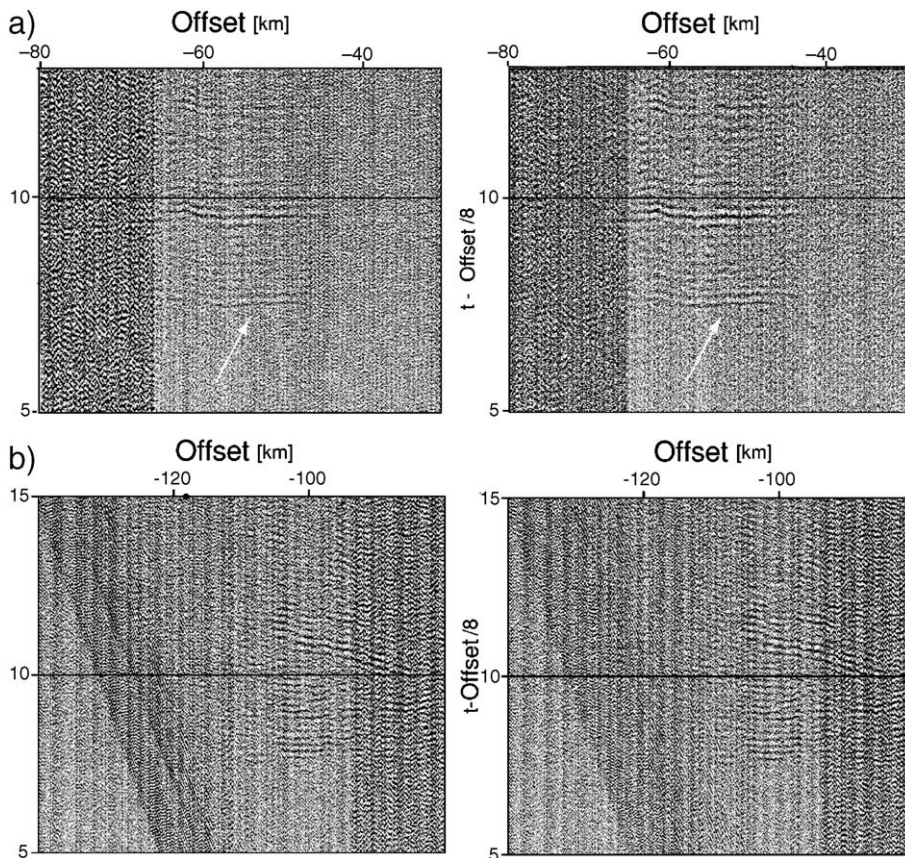

Fig. 2. Example of predictive deconvolution and F–K filtering. (a) The left figure shows a section of the recording of OBH 09, P2 after band-pass filtering (3–25 Hz), showing the Moho refraction. The right figure shows the result after deconvolution. The signal is only slightly enhanced. (b) The left figure shows a section of the recording of OBH 18, P2, after band-pass filtering (3–25 Hz) showing the Moho refraction. The right figure shows the result of the F–K filtering. The wrap-around is significantly reduced, but new arrivals are not revealed.
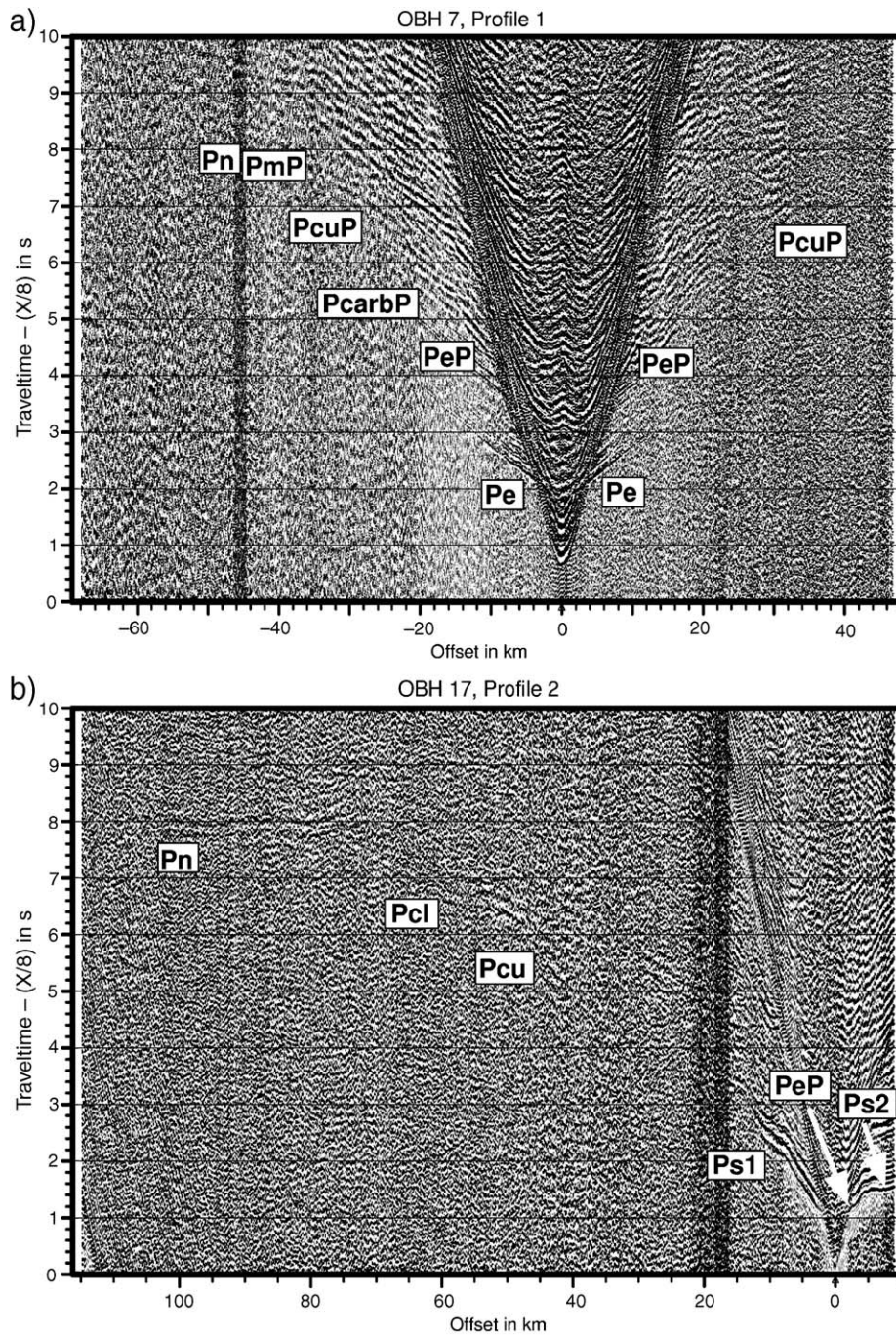
Fig. 3. (a) Recording of OBH 07, P1. The observed arrivals are marked. PeP–reflection from the top of evaporites; Pe–refraction at evaporite layer; PcarbP–reflection from top of carbonate layer; PcuP–reflection from top of upper crust; PmP–Moho reflection; Pn–Moho refraction. (b) Recording of OBH 17, P2. The observed arrivals are marked. PeP reflections from the top of evaporites, Ps1P and Ps2P reflection from top of second layer of Pre-Messinian sediments, Pcu–refraction from the upper crust; Pcl–refraction from the lower crust; Pn–Moho refraction. (c) Recording of OBH 18, P2. The observed arrivals are marked. Ps2P–reflection from top of second layer of Pre-Messinian sediments; PcarbP–reflection from top of carbonate layer; PcuP–reflection from top of upper crust; PclP–reflection from top of lower crust; Pn–Moho refraction.
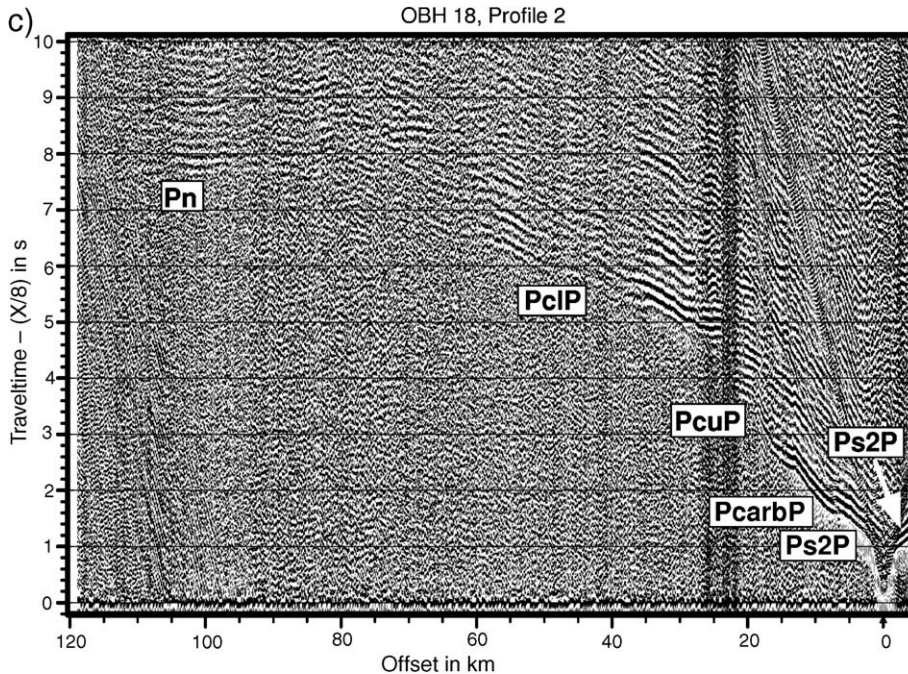
Fig. 3 (*continued*).

arrivals are not observed, the Pe arrivals start at OBH 16 and are present on all other stations basinwards. The PeP only appear on some stations on the slope, on OBH 14, 16, and 17. On line P2, two Pre-Messinian sediment layers are found and the first arrivals at near offsets of Fig. 3c are reflections from the base of the upper sediment layer (Ps2P). Reflections from the upper sediment layer (Ps1P), and turning waves within these layers (Ps1,Ps2) are only observed on a few stations on the slope, owing to the limited extent of the lower sediment layer, and its relatively small thickness on the shelf. The reflection of the top of carbonates (PcarbP) marks the next arrival at 12 km offset. This reflection is observed on seven more stations, diving waves of the carbonate layer (Pcarb) are not recorded on OBH 18, but on three other OBH. At 20 km, the PcuP can be identified on Fig. 3c and farther away the PclP arrival. At an offset of about 80 km, turning waves of the upper mantle arrive (Pn). Pcu, Pcl, and PmP are not be observed on OBH 18. PcuP, Pcu, and PclP are represented on eight, seven, and six stations, respectively, and PmP and Pn on six and five, respectively. Ray coverage of Pcu and PclP arrivals on line P2 are shown in Fig. 4.

The onshore station only recorded signals up to 15 km offset, and only one phase that was identified as PcarbP. There is a lateral transition zone of the marine carbonate layer into a layer of sandstones (Garfunkel, 2004) near the coast, but since this transition could not be resolved on either line, this arrival on the seismic is treated as a reflection from the top of the carbonate layer.

4.3. Seismic reflection data—acquisition

During the cruise M52/2, the amount of 44 multi-channel seismic reflection lines were recorded; two of these coincide with the refraction profiles: line HH02–07 runs along refraction line P1, and HH02–19 runs parallel to P2. Both were recorded with two streamers of 150 m and 600 m active length, respectively. Both streamers
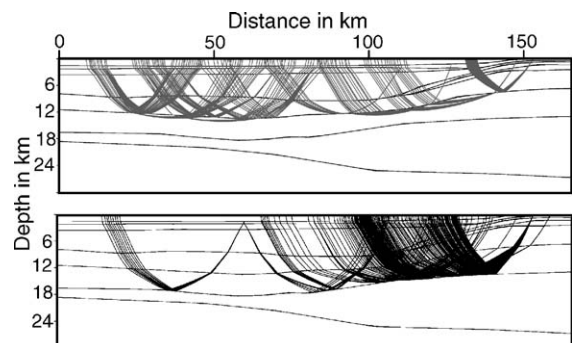

Fig. 4. Example of ray coverage of the upper crust on P2. The upper image shows the refractions within the upper crust recorded by seven stations; the lower image shows reflections form the top of the lower crust recorded by six stations.
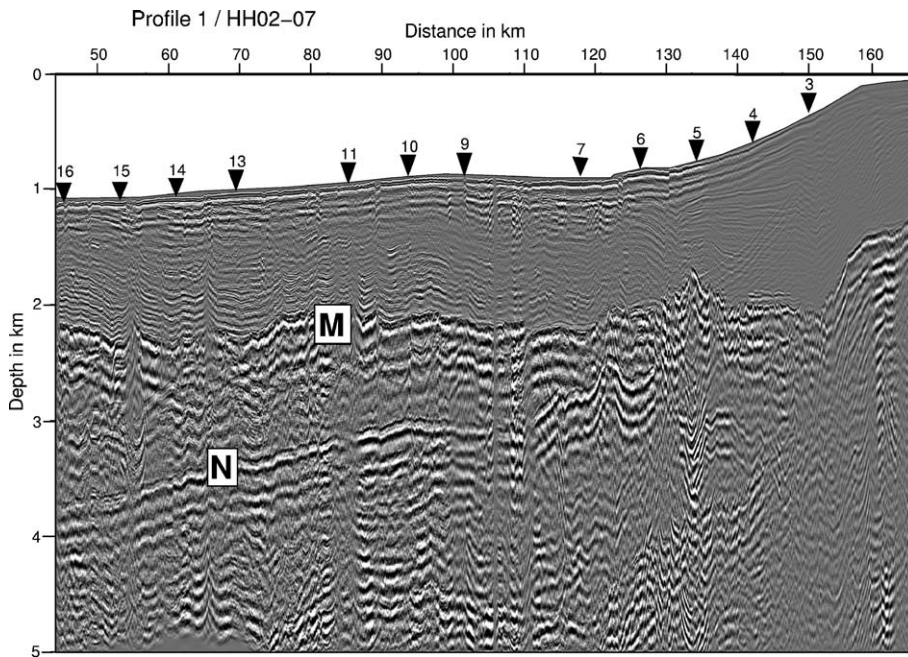
Fig. 5. Model-based depth-migrated section of HH02–07 parallel to P1. Average interval velocities used for the migration were 2.0 km/s for the Plio-Quaternary sediments and 4.2 km/s for the salt layer. M marks the top and N the base of evaporites. Black triangles show the positions of the OBH on line P1.

comprised 24 channels with a group distance of 6.25 m and 25 m, respectively, and a maximum offset of 190 m, and 700 m, respectively. Both recorded with a sampling

rate of 1 ms. The source consisted of two small clusters: one with two GI-Guns, each with a volume of 105 in.[3] operated in the harmonic mode, and the other cluster
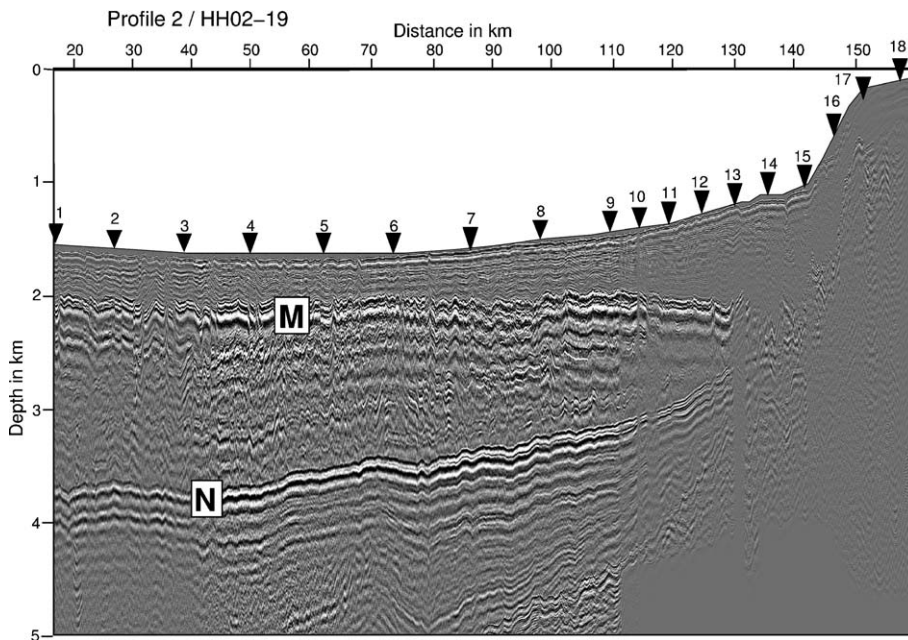

Fig. 6. Model-based depth-migrated section of HH02–19 parallel to P2. Average interval velocities used for the migration were 2.0 km/s for the Plio-Quaternary sediments and 4.2 km/s for the salt layer, as on HH02–07. M marks the top and N the base of evaporites. Black triangles show the positions of the OBH on line P2.

consisting of one GI-Gun with 205/105 in.[3] operated in the airgun mode and a G-Gun of 380 in.[3] (6l). The shot spacing was 25 m (10 s). The airgun array was designed for maximum signal strength accepting a reduced primary to bubble ratio.

4.4. Seismic reflection data—processing and characteristics

The recordings of both streamers were CMP sorted with a CMP spacing of 6.25 m and 12.5 m, respectively, then stacked and band-pass filtered with passing frequencies between 6 and 160 Hz. Only on the recordings of the longer streamer further processing was applied. A stacking velocity analysis was carried out on every 100th CMP in supergathers of 5–9 CMP. The deeper the analysed horizon, the more CMPs were combined to the supergather. The resulting velocity field was smoothed, and the data were time migrated and stacked accordingly. Afterwards, an interval velocity analysis was carried out and a model-based depth migration accomplished. Average interval velocities of post-Messinian sediments and evaporite layer were 2.0 km/s and 4.2 km/s, respectively. Figs. 5 and 6 show the depth-migrated images of line HH02–07 and HH02–19, respectively. On both images the top (M-reflection) and the base (N-reflection) of the salt layer are clearly visible. The M-reflection exhibits a rough surface owing to salt movement and compression (Gradmann et al., 2005), but the N-reflection which represents the Pre-Messinian sea floor is smooth. On line HH02–07, which corresponds to line P1, the sediment thickness of roughly 1 km is almost constant in the basin. N rises gently towards the shelf, but is severely contorted between km 105 and the salt pinch-out. Near the location of OBH 05, a structure can be observed that effects both top and base of the evaporites, N is bent downwards and M upwards. The pinch-out of the evaporites is not very distinct, but probably near the position of OBH 03. On line HH02–19 (Fig. 6) corresponding to line P2, the sediment layer is significantly thinner, it is only about 0.5 km thick, and shows a clear thickening on the bottom of the slope. The salt layer is slightly thicker than on line HH02–07 and does not exhibit any significant contortion of N. The pinch-out is even more disguised than on line HH02–07, but is assumed to occur near the location of OBH 15.

4.5. Gravity data

Gravity data were continuously recorded along the entire ship track in the research area, thus, also along the two refraction lines. Gravity values were measured with the Gravity Meter System KSS30/31 and instantly converted into free-air anomaly values.

5. Modelling of refraction data

On line P1, 13 stations were used for ray-tracing; on P2, all 19 stations were suitable for the modeling. The land station at the end of line P2 was also included. The modeling was performed with the software package rayinvr of Zelt and Smith (1992). The depth-migrated images of line HH02–07 and HH02–19 served as starting models for the uppermost sediments and the top and base of the salt layer. Suitable uncertainty values (error bars) were assigned to all traveltime picks: Depending on the S/N ratio and the phase correlation quality, uncertainties between 0.020 and 0.125 s were assigned (Table 1). First, a forward modeling technique was applied, in which the modeling took place layer by layer. Velocity and depth nodes were held fixed, when the next, deeper layer was modeled. Improved traveltime fits come with the

Table 1

Phase	Points used	Uncertainty (s)	Traveltime misfit (s)	χ^2
Line P1				
Pw	430	0.020–0.125	0.079	2.087
PeP	276	0.020–0.125	0.094	1.502
Pe	553	0.035–0.125	0.070	1.145
PcarbP	139	0.035–0.075	0.056	0.826
PcuP	109	0.035–0.080	0.084	1.196
PclP	28	0.050–0.100	0.089	0.988
PmP	87	0.035–0.100	0.085	0.864
Pn	56	0.050–0.125	0.077	0.800
Entire model	1678	–	0.078	1.389
Line P2				
Pw	754	0.050–0.100	0.080	2.353
PeP	18	0.035–0.100	0.133	2.391
Pe	708	0.035–0.125	0.073	1.043
PsuP	63	0.035–0.125	0.113	2.297
Psu	5	0.100	0.164	3.359
PslP	190	0.035–0.125	0.091	1.112
PcarbP	80	0.050–0.125	0.204	6.247
Pcarb	45	0.075–0.125	0.149	1.758
PcuP	161	0.035–0.125	0.222	5.305
Pcu	63	0.050–0.125	0.121	0.988
PclP	222	0.075–0.125	0.154	1.591
Pcl	27	0.050–0.125	0.178	2.727
PmP	112	0.050–0.125	0.198	2.636
Pn	317	0.050–0.125	0.145	1.837
Entire model	2765	–	0.123	2.059

addition of nodes in the model. However, because of the sparse ray coverage in some areas, it was also an aim not to over-fit the model by adding too many nodes that would be poorly constrained. Exempt were nodes that were confined by the depth migrated MCS data, e.g., the undulation in the top of salt layer at approximately 135 km and in the base of this layer at about 120 km. The final models of both lines were derived by application of the inversion method of rayinvr. Ray-tracing examples of four stations of each line are shown in Figs. 7 and 8. They show the good fit of the observed and calculated traveltimes and the generally dense sampling by the rays.

5.1. Resolution and uncertainty of the modeled velocity structure

The reliability of the final velocity structure is expressed in the resolution calculated by the inversion algorithm of rayinvr (Zelt and Smith, 1992). This quantitative approach is based on the relative number of rays which determine the parameterization of the model, i.e., the velocity nodes. According to Zelt and Smith (1992), resolution values of 0.5 or greater are considered to be well resolved. A resolution is calculated for each velocity node in the final model and then interpolated onto a 2.5×0.25-km grid (Figs. 9 and 10), velocity and
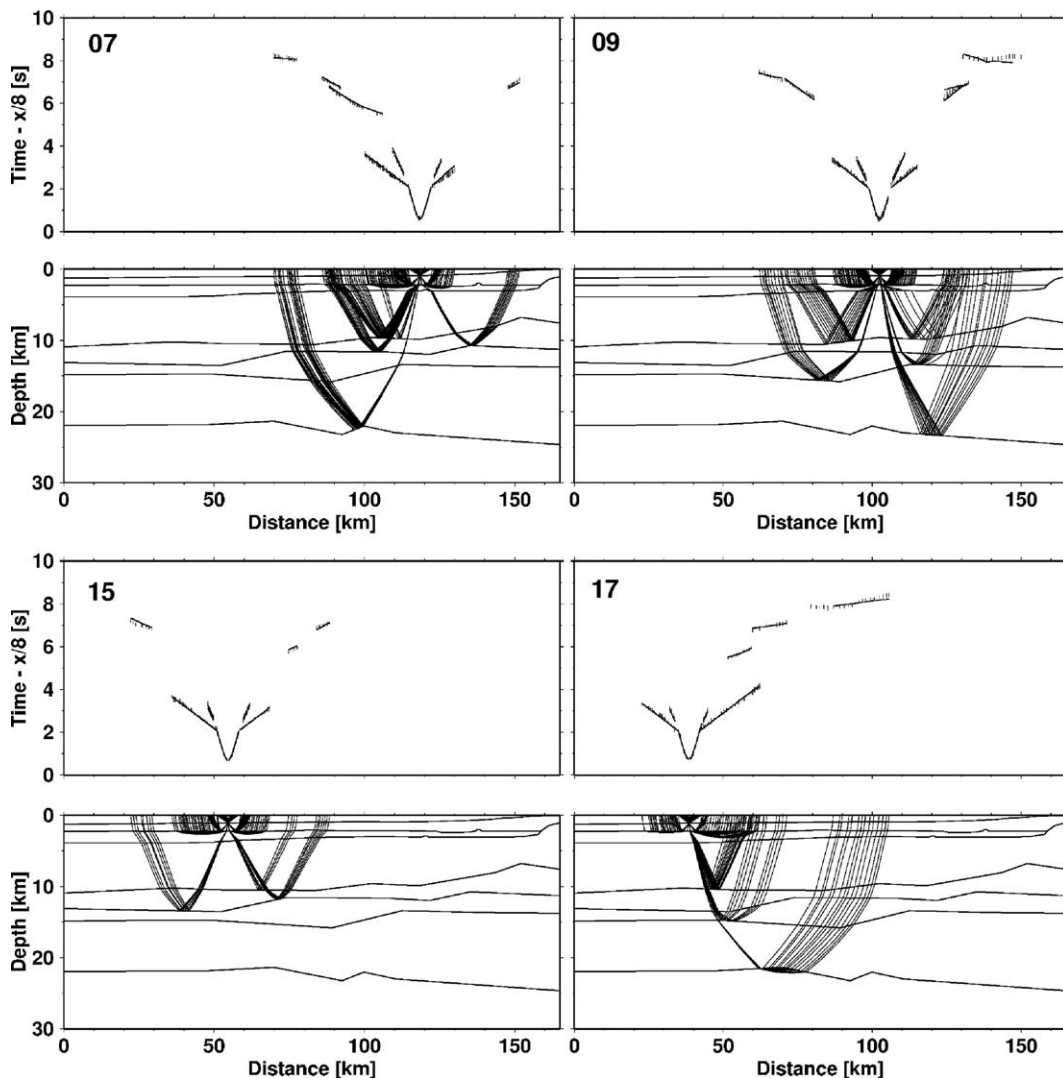

Fig. 7. Examples of ray-tracing along Profile P1 from stations 07, 09, 15, 17. These stations cover different parts of the model. The upper parts show the observed and calculated P-wave arrivals. Gray error bars indicate the assigned error to the picked traveltimes. Black lines show the traveltimes calculated using the final velocity model shown in Fig. 11. The lower parts are respective paths for rays calculated by rayinvr.
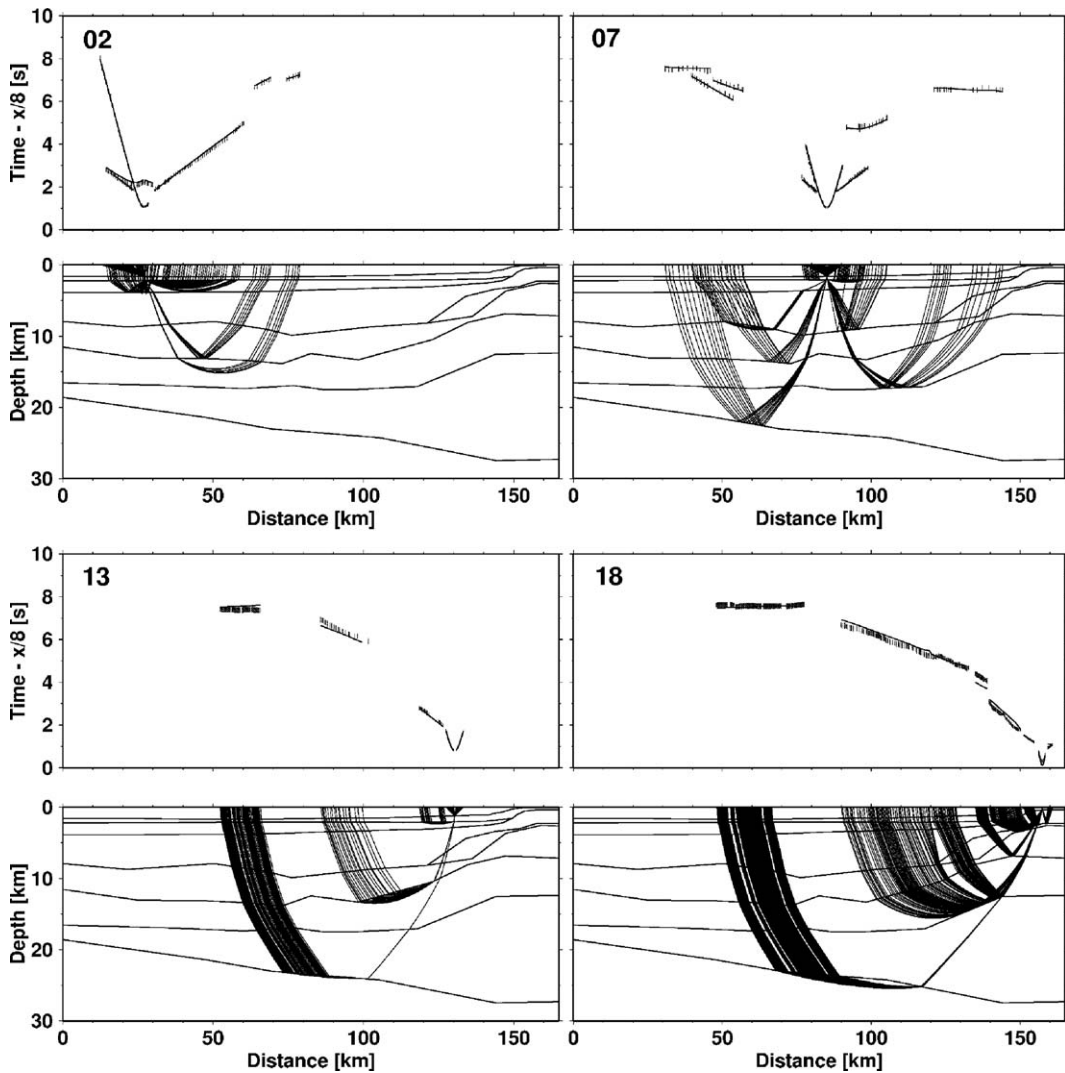
Fig. 8. Examples of ray-tracing along Profile P2 from stations 02, 07, 13 and 18. The upper parts again show the observed and calculated P-wave arrivals. Gray error bars indicate the assigned error to the picked traveltimes. Black lines show the traveltimes calculated using the final velocity model shown in Fig. 12. The lower parts are respective paths for rays calculated by rayinvr.

boundary uncertainty were set to 0.2 km/s and 0.5 km, respectively. The resulting calculated resolution of the model of profile P1 is shown in Fig. 9. It reveals a moderate resolution down to the top of the carbonate layer, but poor resolution below, except for a small part of the lower crust. One way to enhance resolution is to limit the number of nodes, but since the number of velocity nodes in both crustal layers and the carbonate layer was already reduced to five, the resolution of this model could not be improved any further. The resolution of the model of profile P2 is shown in Fig. 10. Here, the resolution is satisfying throughout the model, with the exception of the edges and a part of the carbonate and the lower sediment layer.

Further constraints on the reliability of the velocity models are given by the rms-traveltime misfit and the χ^2-normalized misfit parameter provided by rayinvr. The number of used picks, the rms-traveltime misfit and the χ^2-values are given in Table 1. An χ^2-value equal to 1 indicates that the data are fitted within their assigned uncertainties. χ^2-values smaller than 1 refer to the presence of structures in the model not required by traveltime picks. This occurs mainly at the PmP and Pn of line P1 because of the small number of picks. According to Zelt and Smith (1992) small-scale heterogeneities and significant out-of-plane structural and velocity variations can increase χ^2. According to Hirsch et al. (1995) and Vidal et al. (2000a,b), the
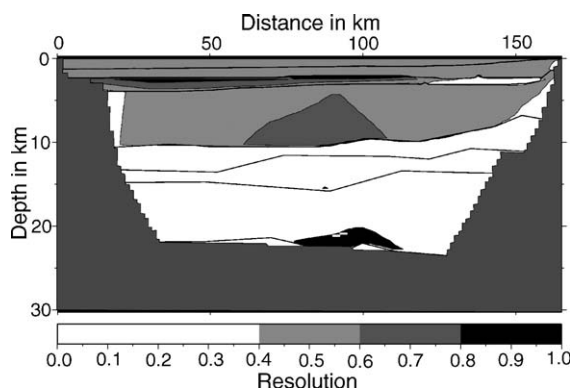
Fig. 9. Resolution of final P-wave velocity model of P1 calculated by rayinvr. Resolution is shown in gray-shade intervals. The resolution values represent the values of the main diagonal of the resolution matrix of the p-wave velocity–depth model. Maximum resolution is represented by the value of 1. Smaller values denote a spatial averaging of the true earth by a linear combination of model parameters (Zelt, 1999). According to (Zelt and Smith 1992), resolution values greater than 0.5 are considered well resolved and reliable, although this is only an empiric value.

basement and the carbonate layer up to the Neogene sediments are noticeably faulted with significant vertical displacements. Such displacements cannot be resolved and lead to an increased χ^2. In this context, the values in this study can be regarded as acceptable. Generally, stations on the slope produce a higher misfit than stations in the basin. On P2, the highest χ^2-values are reached at OBH 15 with 4.085, but most of the stations (01, 02, 03, 04, 05, 06, 07, 10, 11, 12, 13, 19 and the land station) achieve a χ^2-value under 2.3.

6. Results

6.1. Profile 1

The model (Fig. 11) shows a layer of Plio-Quaternary sediments of 1.9–2.1 km/s above the evaporite layer with 4.3–4.4 km/s, as was already shown on the MCS lines. Under these layers, older sediments from Jurassic to Miocene are located with velocities from 3.5 to 3.9 km/s. These sediments are underlain by a layer of 4.4–4.8 km/s, respectively. This layer has been observed before (Ben-Avraham et al., 2002) and has been identified as marine carbonates that are interbedded with sandstones near the shelf (Garfunkel, 2004). Two crustal layers are present throughout the model, the upper crust with 6.0–6.2 km/s and the lower crust with 6.4–6.8 km/s. The Moho lies at 22–23 km depth and the velocity of the uppermost mantle is determined to 7.8 km/s.

Small bulges are located at the top of the evaporite layer at 138 km and at the base at 120 km. These are below the resolution limit, but were observed on the MCS line and included in the model. The bulge in the top of salt may be related to salt tectonics, but the one at the base of salt is an indication of deeper tectonic activity. The Pre-Messinian sediments show a change in velocity at 90 and 110 km, and at 25 km. At 25 km, the velocity of the entire sediment package is reduced by ca. 200 m/s; at 110 km, only the upper section is involved, and the velocity at the base of the sediments is not affected. The velocity variation at 90 km also involves the whole layer; here, the velocity gradient is significantly changed, and the velocity stays almost constant from the top to the base of this layer. The carbonate layer and the crust exhibiting an otherwise uniform velocity distribution also comprise a zone with reduced velocity at 90 km. Thus, this zone of reduced velocity extends from 4 km depth down to the Moho at 23 km. The gravity model shows a steep decline of the Moho under the shelf.

6.2. Profile 2

The model of P2 (Fig. 12) shows a very similar layering to the model of P1. The Pre-Jurassic sediments have a slightly higher P-wave velocity of 3.7–4.4 km/s with a steeper velocity gradient. P2 also contains a second sediment layer with 4.5–4.6 km/s that forms a wedge at the bottom of the slope. The velocity of the carbonate layer is also higher with 4.6–4.9 km/s. Both crustal layers that appear in line P1, the upper crust with 5.7–6.4 km/s and the lower crust with 6.6–6.9 km/s are observed on profile P2. The velocities of the crustal layers are generally higher in P1 by about 100 m/s, and
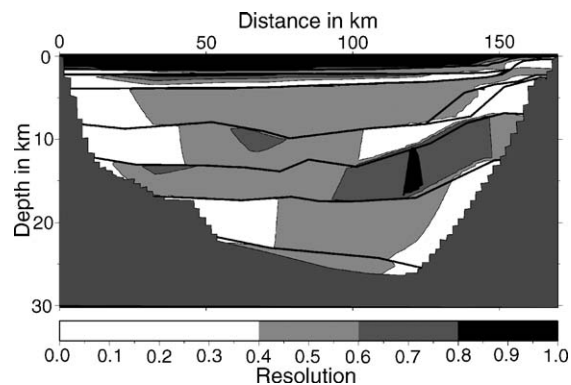

Fig. 10. Resolution of final P-wave velocity model of P1 calculated by rayinvr. Resolution is shown in grayshade intervals. See Fig. 9 for explanation.
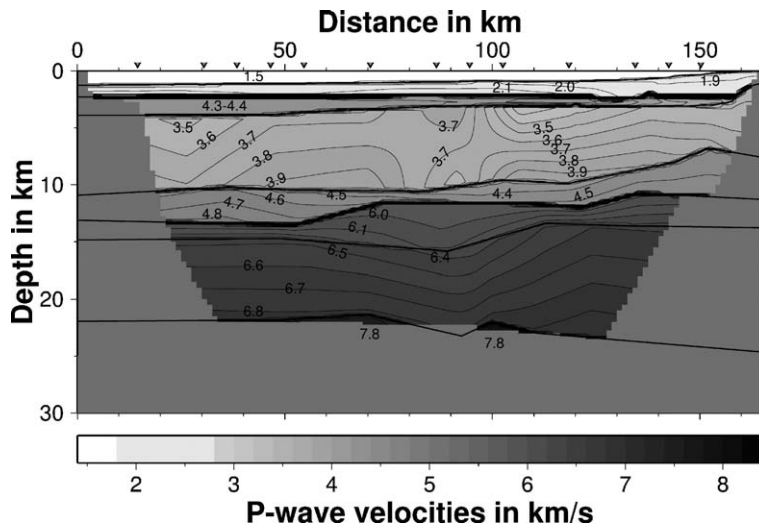
Fig. 11. Final velocity model of line P1. Velocities (in km/s) are indicated by gray shades and contour lines where constrained by ray coverage. Thick black lines represent layer boundaries. Triangles mark positions of the OBH.

the upper crust shows a steeper gradient. The Moho decreases from 22 to 26 km. The uppermost mantle exhibits a velocity of 7.8–7.9 km/s.

All layers show a uniform velocity distribution; only in the upper section of the Pre-Messinian sediments, a variation in the velocity gradient is observed at 95 km. A very small velocity variation is observed at 75 km in the carbonate layer, accompanied by an unevenness in the boundaries of carbonates and upper crust. Unlike the model of P1, a significant thickening of the crust towards the shelf can be seen. This thickening takes place mainly in the lower crust, but also the upper crust increases its thickness from 4 km in the basin to 6 km near the edge of the model.

6.3. Gravity models

In order to provide a further constraint on the crustal structure, free air gravity modelling was carried out along both lines P1 and P2. The deduced density models are based on the results of the velocity models
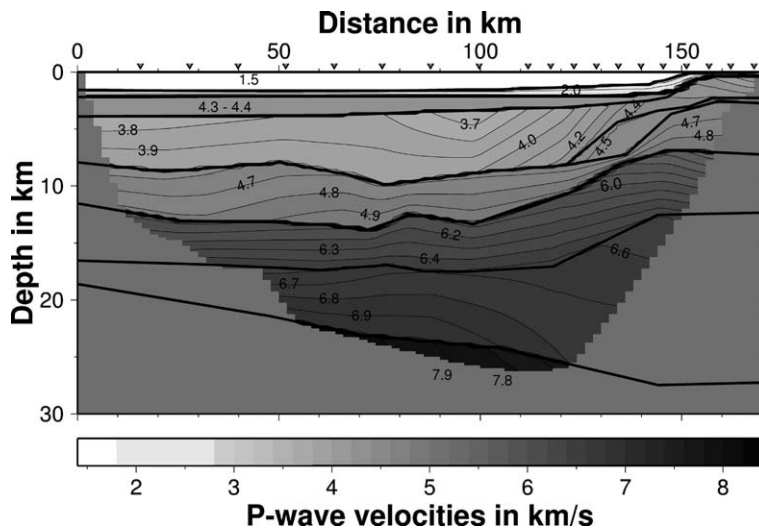

Fig. 12. Final velocity model of line P2. Velocities (in km/s) are indicated by gray shades and contour lines where constrained by ray coverage. Thick black lines represent layer boundaries. Triangles mark positions of the OBH.

using common velocity–density relationships (e.g., Nafe and Drake, 1963). The modelling was carried out using a 2-D modelling program based on Talwani et al. (1959). For both models, the layer boundaries were kept fixed where constrained by seismic data. The misfit between observed and modelled free air anomaly is less than 10 mGal. This maximum misfit might seem large, but a look on a free air anomaly map of the Levantine Basin, based on satellite data from Sandwell and Smith (1997) shows that large anomalies lie off the lines P1 and P2 or run obliquely to the profiles (Fig. 13). Therefore, a 2-D approach in gravity modelling can only yield limited accuracy. The density model of P1 (Fig. 14) confirms the velocity model. In

order to fit the local minimum at 60 km, an additional sediment block had to be modelled. Because of the short wavelength of this minimum, it could not be caused by a deeper body, e.g., in the crust. Toward the end of the line, the thickness of both upper and lower crust has to increase to match the observed gravity values and compensate the effects of the shelf. On line P2 (Fig. 15), in comparison, free air gravity significantly increases at the end of the model and follows the bathymetry. On this line, crustal thickening already occurs in the center of the model, also visible in the velocity model. The additional sediment body in the velocity model near the shelf was modelled together with the other Pre-Messinian sediments as one layer,
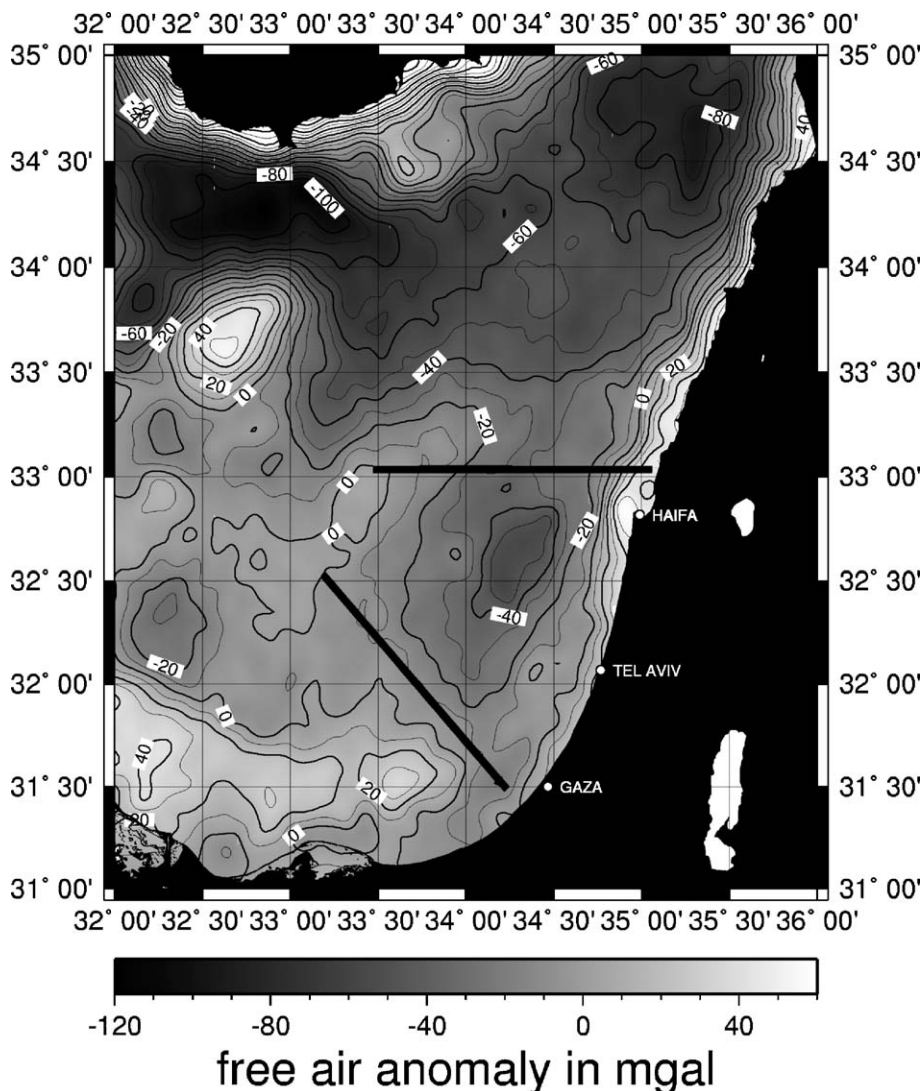

Fig. 13. Free air anomaly map of the Levantine Basin, based on satellite data of Sandwell and Smith (1997). Solid lines mark the positions of profiles P1 and P2.
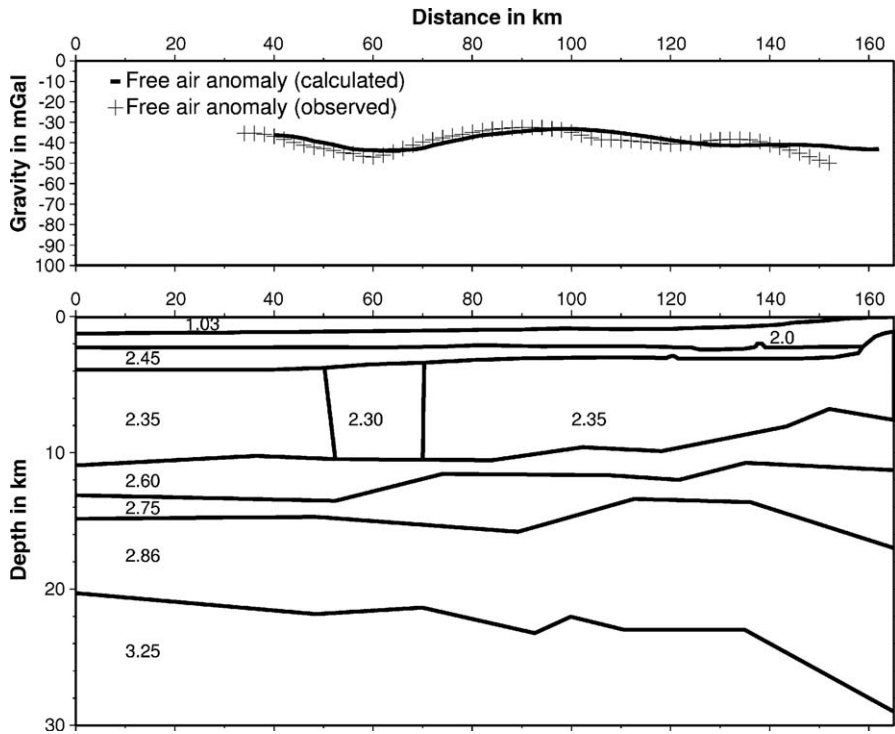
Fig. 14. Upper part shows observed (+) and calculated (−) free air anomaly, based on the final 2D density model of P1 shown in the lower part. Layer boundaries were retained from velocity model where constrained by ray coverage. Maximum misfit is <10 mGal.
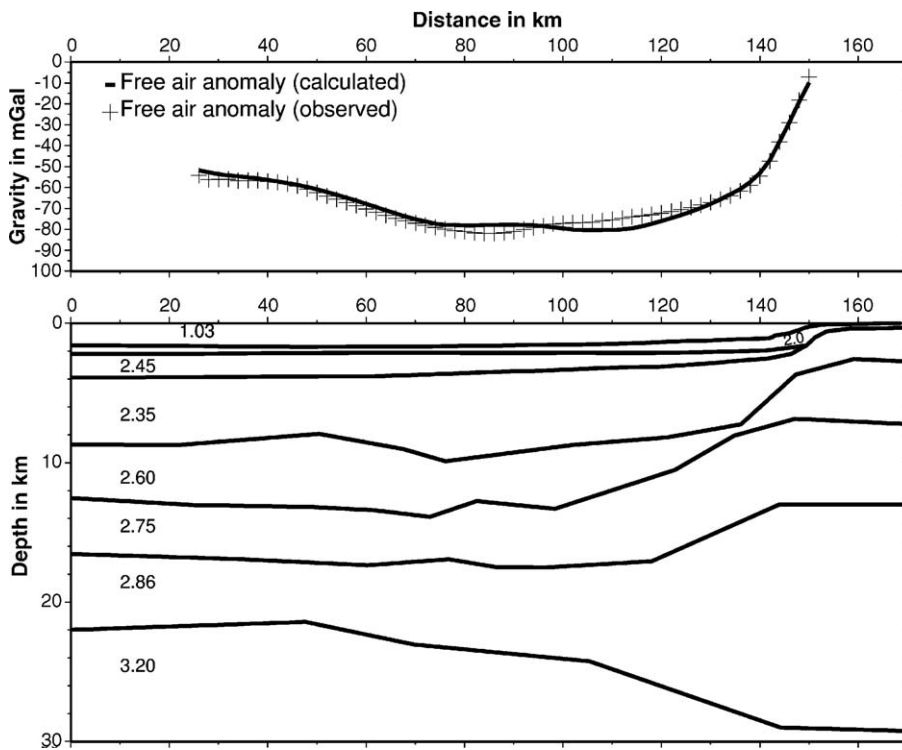

Fig. 15. Upper part shows observed (+) and calculated (−) free air anomaly, based on the final 2D density model of P2 shown in the lower part. Layer boundaries were retained from velocity model where constrained by ray coverage. Maximum misfit is <10 mGal.

since the best gravity fit was obtained with the same densities of both bodies.

7. Discussion

7.1. Velocity distribution and crustal structure

On line P1 lateral changes in the velocity gradient in the Pre-Messinian sediments are observed at 25 km, 90 km, and at 110 km. The change at 90 km, which also appears in the crust, coincides with the projection of the Pelusium Line on P1, and the change at 25 km coincides with the location of the Damietta–Latakia Line. The variation in the velocity structure at 110 km is not clearly associated with any known fault line or other structure.

On line P2, only one distinct change in the velocity gradient appears at 95 km. On the map of Neev et al. (1976), the Damietta–Latakia Line would meet the profile at approximately 75 km. An earthquake lineament runs along this line starting from about 33°N and continuing towards the Cyprus Arc (Fig. 1). At 75 km, only small velocity and boundary undulations are observed. These undulations are likely to be an effect of the Damietta–Latakia Line.

The Pelusium Line is projected to meet line P2 between 130 and 140 km. Here, no velocity effects are visible. But at 120 km, the slope of the deeper sediment layers begins, so any velocity variation owing to the Pelusium Line might be masked by the slope and its steep layer boundaries. To sum up, indication of the known shear zones, Pelusium and Damietta–Latakia Line, are observed on both lines, although they are more pronounced on line P1. We also found evidence of shearing in yet unpublished industrial MCS data of the Levantine Basin. Since shear zones are much more common in continental than in oceanic crust, this is a first indication of continental crust in the Levantine Basin.

Generally, the velocities of the lower crust cannot be classified as either typical for oceanic or continental crust, but with 6.4–6.9 km/s, they would be remarkably low for oceanic crust, especially if–for oceanic crust– the anomalously great depth and resulting pressure is considered. In theory, increased heat flux and higher crustal temperature might decrease the velocities in the lower crust. Heat flow maps of the Eastern Mediterranean Sea (Makris and Stobbe, 1984; Jiménez-Munt et al., 2003) do not show increased heat flow values in the Levantine Basin. Heat flow values range between 40 and 60 mW/m^2 (Jiménez-Munt et al., 2003) and 38–67 mW/m^2 (Makris and Stobbe, 1984); sediments account for approximately additional 12 mW/m^2 (Ben-Avraham et al., 2002). This complies as well with the average heat flow value of 51–62 mW/m^2 given for oceanic crust of Late Jurassic to Late Cretaceous age (Pollack et al., 1993), as expected for the Levantine Basin. But it complies just as well with the average heat flow value of 65 mW/m^2 for continental crust (Pollack et al., 1993). Hence, the heat flow values are not specific of either type of crust, but a decrease of velocity in the lower crust due to thermal sources and increased crustal temperature can be excluded and no correction to the velocity of the lower crust need to be applied. Therefore, the velocity of the lower crust more likely supports the assumption of continental crust.

The crustal velocities found onshore by Ben-Avraham et al. (2002) only slightly south of line P2 and the crustal velocities of line P2 are in good agreement. Ben-Avraham et al. (2002) find an average P-wave velocity of 6.3 km/s in the upper and 6.7 km/s in the lower crust, which match the 6.0–6.4 km/s in the upper crust of line P2 and the 6.6–6.9 km/s in the lower crust. A compilation of the results of the DESERT2000-project (Weber et al., 2004), profile III of the study of Ben-Avraham et al. (2002) and our line P1 (Fig. 16), which are almost in line (Fig. 1), reveal a very good match between the crustal structure and velocities under Israel and Jordan and the model of P1. The continuation with profile III of Ben-Avraham et al. (2002) shows a matching Moho depth, but there is only one crustal layer that was detected. Since the study of Ben-Avraham et al. (2002) was based on fewer receivers and greater receiver spacing, the velocity models derived in our study should be considered as more reliable. Fig. 4 shows the ray coverage of the upper crust on line P2. It shows not only reflections from the boundary between the upper and the lower crust, but also rays which are refracted within the upper crust. The arrivals corresponding to these rays are directly related to the p-wave velocity in the upper crust and confirm the presence of a layer with another p-wave velocity than that in the lower crust. Therefore, a velocity model with two crustal layers fits our data much better than only one crustal layer.

The crustal velocities found on the DESERT2000-line are 6.1–6.4 km/s in the upper crust and 6.7 km/s in the lower crust. These are slightly higher than the velocities on line P1 with 6.0–6.2 km/s and 6.5–6.8 km/s, and slightly lower than on line P2 with up to 6.4 km/s in the upper and 6.6–6.9 km/s in the lower crust, which can be considered a good match and further supports the hypothesis of continental crust extending into the Levantine Basin.

The thickness ratio of upper crust to lower crust varies between 1:3 and 2:5 on line P1 and 1:2 and 2:3 on
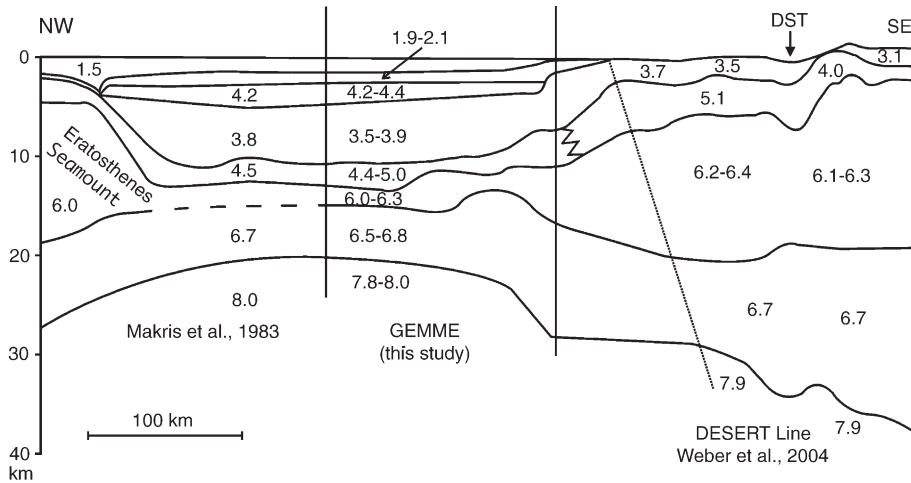
Fig. 16. Compilation model from Eratosthenes Seamount over Levantine Basin into Jordan, based on the previous velocity model of Makris et al. (1983), the crustal model of the DESERT2000-line and line P1 of this study (see Fig. 1 for location). Dashed line marks suggested continuation of intercrustal layer boundary observed on P1 and DESERT2000-line, but not in the model of Makris et al. (1983). Dotted lines mark the limits of each survey, vertical zigzag indicates transition from marine carbonates to sandstone.

line P2. However, with an uncertainty of 0.5 km and thicknesses of 2–4 km in the upper crust and 6–9 km in the lower crust, the uncertainty in the thickness ratio reaches up to 70%. Considering this, and taking into account that the resolution values in the crust of line P1 is relatively low, any considerations of changes in the thickness ratio and crustal flow are futile.

The Moho depth lies between 22 and 26 km and the combined thickness of both layers varies between 8 and 18 km. Although in the seismic survey of Makris et al. (1983) and Ben-Avraham et al. (2002), only one crustal layer could be detected, the same Moho depths were found. Based on 1-D velocity–depth profiles yielding different Moho depths under Judea–Samaria and Galilee–Lebanon (Fig. 17) different velocities in the upper crust with 6.0 km/s and a Moho depth of 20 km and 6.3 km/s and 25 km, respectively, Ben-Avraham and Ginzburg (1990) suggested that these were different terrains. In our study, the average velocities of the upper crust are about 6.1 and 6.2 km/s on P1 and P2, respectively. This small difference does not point at the existence of different crustal blocks or terrains in the basin.

Although the crustal structure resulting from this study can neither be classified as typically oceanic nor as typically continental, it is comparable with other areas of thinned continental crust in the Mediterranean Sea (Fig. 17). Bohnhoff et al. (2001) analysed three seismic refraction profiles in the southern Aegean across Crete and found continental crust under Santorini and further south, with a Moho depth between 15 and 33 km and a crustal thickness of approximately 13 km. The crust

under Santorini consists of two layers with velocities between 6.0–6.4 km/s in the upper crust and 6.5–6.9 km/s in the lower crust, which is comparable to our results. A seismic refraction survey of Makris et al. (2001) in central Greece yielded a similar crustal structure, they also find thinned continental crust, with a Moho depth as low as 18 km, a crustal thickness of 13 km overlain by sediment layers of several kilometers thickness. The velocities of the upper and lower crust are specified as 6.0–6.3 km/s and 6.5–6.8 km/s, respectively, and the ratio in thickness of upper to lower crust varies between 2:3 and 2:5. Peirce and Barton (1992) analysed a refraction seismic profile in the Sardinia Channel as part of the European Geotraverse program. They found only one crustal layer between Sardinia and Tunisia thinning from 24 to 10 km in thickness with a central Moho depth of 18 km and identified it as thinned continental crust. Generally, the continental crust in the Mediterranean Sea seems to consist of not more than two layers. Outside the Mediterranean Sea, in the Galicia Interior Basin offshore Portugal, at a rifted non-volcanic margin, Pérez-Gussinyé et al. (2003) find thinned continental crust which exhibits a transition in crustal structure from three layers to two layers. They interpret this transition as a suture separating two terrains with different crustal characteristics. Hauser et al. (1995) find such a transition from a three-layer to a two-layer crust in the Rockall Trough and offer another explanation for the disappearance of a third crustal layer. They postulate that the stretching of the crust modifies it and causes amalgamation of the upper and the middle crust into only one seismically detectable layer. Since
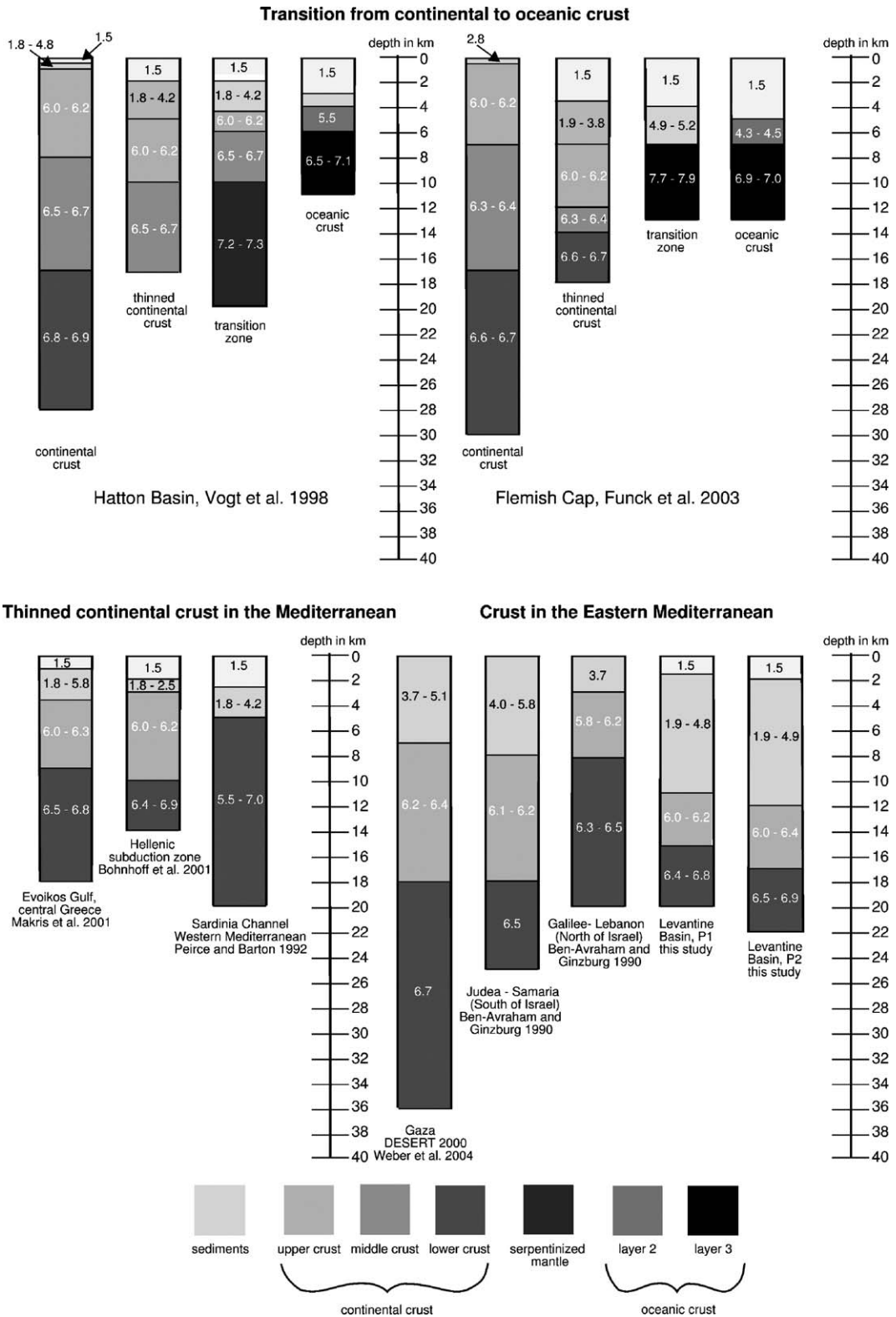
Fig. 17. Compilation of 1D velocity–depth profiles. The numbers denote p-wave velocities in kilometers per second. Top: examples of transitions from continental to oceanic crust. Bottom left: examples of thinned continental crust in the Mediterranean Sea. Bottom right: velocity–depth profiles of the Levantine Basin and adjacent areas.

throughout the Mediterranean Sea, strongly attenuated continental crust is found, it is conceivable that this crust had been structured in three layers, but has been modified by thinning into a crustal composition of two layers.

The assumption of oceanic crust requires a transition from continental to oceanic crust. An abrupt transition is not observed on either line, but the rise of the Moho from 26 to 22 km on line P2 and from 27 km (Weber et al., 2004) near Gaza to 22 km on line P1 could mark a zone with a gradual transition from continental to oceanic crust. Such a transition zone has been observed elsewhere, e.g., at the Hatton margin offshore Ireland (Vogt et al., 1998), at the Flemish Cap off New Foundland (Funck et al., 2004) and in Nova Scotia (Funck et al., 2004). In Nova Scotia and at the Flemish Cap ,the transition zones are characterized by an extremely thinned crust of 2–3 km overlying serpentinized mantle with 7.2–7.6 km/s (Nova Scotia) or 7.7–7.9 km/s (Flemish Cap). This layer is significantly faster than the lower continental crust with 6.6–6.9 km/s. Also, a strong decrease of Moho depth from 30 to 10 km (Flemish Cap) and 37 to 13 km (Nova Scotia) is observed. At the Hatton margin, crustal thinning from 20 to 5 km is observed along with a decrease in Moho depth from 22 to 12 km (Fig. 17). Under the extremely thinned crust, magmatic underplating has taken place, and the underplated body has a velocity of 7.2–7.3 km/s compared to 6.8–6.9 km/s of the lower crust. Common features of these three transition zones from continental to oceanic crust are extremely thinned crust of only a few kilometers above a layer with a velocity >7.0 km/s, higher than the velocity of the adjacent lower continental crust and a distinct decrease in Moho depth. In both the models of P1 and P2, neither a body with a velocity >7.0 km/s nor extremely thinned crust of 5 km or less are observed. The comparatively gentle rise of the Moho from 27 to 22 km, the decrease in thickness from 18 to 8 km and the stable velocity gradient from 6.4 to 6.8 km/s (P1) and 6.5 to 6.9 km/s (P2) show little similarity to the transition zones seen at Nova Scotia, at the Flemish Cap or at the Hatton margin. They rather suggest continuous thinned continental crust in the Levantine Basin. Comparison with the Galicia Interior Basin (Pérez-Gussinyé et al., 2003), where the Moho depth decreases from 22 to 14 km, and the crustal thickness from 18 to 8 km, but the velocity stays constant with 6.6–6.9 km/s, reveals much more similarity with the Levantine Basin and suggests that in the Levantine Basin, similar to the Galicia Interior Basin rifting took place, but the stage of continental breakup and sea-floor spreading was not reached.

7.2. β-factor

The stretching factor (β-factor) is defined as the ratio between the crustal thickness before and after stretching. On both lines P1 and P2, the crust thins to a thickness of 8 km, but the β-factor strongly depends on the initial thickness. Taking the present crustal thickness of 18 km under Galilee or Judea–Samaria (Ben-Avraham et al., 2002), the resulting β-factor would be 2.25, but according to Weber et al. (2004), the crustal thickness increases continuously from Israel into Jordan to almost 40 km (Fig. 17). Considering 40 km as the initial thickness and assuming that the crust under Galilee is already thinned, the β-factor increases to 5. A β-factor of >2 is found in several regions in the Mediterranean Sea. Peirce and Barton (1992) find a decrease of crustal thickness in the Sardinia Channel from 24 to 10 km, which would yield a β-factor of 2.4, Bohnhoff et al. (2001) find the crust near Crete thinning from 28 to 13 km, yielding a β-factor of 2.2, and according to Makris et al. (2001), the crustal thickness decreases from 27 to 13 km in the Evoikos Gulf in Central Greece, which results in a β-factor of 2.1. Comparing these results with the Levantine Basin, a β-factor of 2.25 seems reasonable and not unusual.

A β-factor as high as 5 can also be found in other regions, e.g., Hauser et al. (1995) found a β-factor of 4–6 in the Rockall Trough offshore Ireland, assuming an initial crustal thickness of 30 km. Funck et al. (2004) calculated a β-factor of 4.4 with an initial thickness of 35 km in Nova Scotia, and Pérez-Gussinyé et al. (2003) found a β-factor of even 5.3 in the Galicia Interior Basin. These comparisons show that even an assumption of 40 km initial crustal thickness and the resulting β-factor of 5 in the Levantine Basin do not rule out the possibility of thinned continental crust. Taking the present 18-km crustal thickness under Galilee as the initial thickness, the resulting β-factor of 2.25 would even classify as typical for thinned continental crust in the Mediterranean region.

7.3. Implications

Accepting the hypothesis of continental crust in the Levantine Basin allows the following considerations: According to Buck (1991), continental lithospheric extension can be divided into three modes: the narrow rift mode, the wide rift mode and the core complex mode. The narrow rift mode is characterized by a narrow region (<100 km) of extensional faulting, a large lateral gradient in crustal thickness, a low initial heat flow of approximately 60 mW/m^2, and a Moho temperature of

$< 750\,°C$. In the wide rift mode, the region of extension can be as large as 800 km, the lateral gradient in crustal thickness is small, the initial heat flow approximately $80\,mW/m^2$, and the Moho temperature is $> 750\,°C$. The core complex mode results from extension at a high strain rate over a narrow (< 100 km) region and a high initial heat flow of $100\,mW/m^2$, accompanied by a very high Moho temperature.

Considering the distance of maximum 250 km between the continental fragment of the Eratosthenes Seamount and the Israeli margin, the region of the rifting in the Levantine Basin must have been narrow. Extensional faults are not resolved in the velocity models and are masked by salt tectonics in MCS lines, but Hirsch et al. (1995) show extensional faults over a range of ≈ 110 km. Although on both P1 and P2 rather small lateral gradients in crustal thickness are observed, these findings tentatively support the assumption of extension in the narrow rift mode in the Levantine Basin. Therewith, the heat flow at the time of extension was probably not significantly higher than presently, 50–$60\,mW/m^2$.

Pérez-Gussinyé et al. (2003) suggest a deformation model for the Galicia Interior Basin with an initially cold and thin crust, where at the beginning of the rifting, the upper rocks deformed brittlely and the lower crustal rocks ductilly without significant lower crustal flow. With $\beta < 2$, the ratio in thickness of upper to lower crust stays constant, and the extension occurred by pure shear. With increasing extension, lower crustal rocks cooled, changed from plastic to brittle deformation, and at $\beta > 3.5$, faults began to reach into the crust and on a small-scale lower crustal flow started in the direction opposite to fault dip. The extrapolation of $\beta > 5$ yields purely brittle deformation of the crust, faults reaching into the mantle and leading to serpentinization. In order to explain the faults in the crust observed by Hirsch et al. (1995), an intermediate β-factor of ~ 3 would be required according to Pérez-Gussinyé et al. (2003), corresponding an initial crustal thickness of 24 km. Since we do not have any further constraints, e.g., on the rheology of the crust, a detailed analysis of the rifting process is left to speculation. However, based on our interpretation of continental crust in the Levantine Basin, we suggest a modification of the paleo-reconstruction of Garfunkel (1998) (Fig. 18a and b). The Paleo-Tethys is subducted in the Late Permian (Fig. 18a). Two stages of rifting follow, the first from Late Permian to Early Triassic, the second from Late Triassic to Early Jurassic (Walley, 1998). In the late Triassic, the rifting axis running E–W develops to a sea-floor spreading axis opening the Neo-Tethys, and oceanic
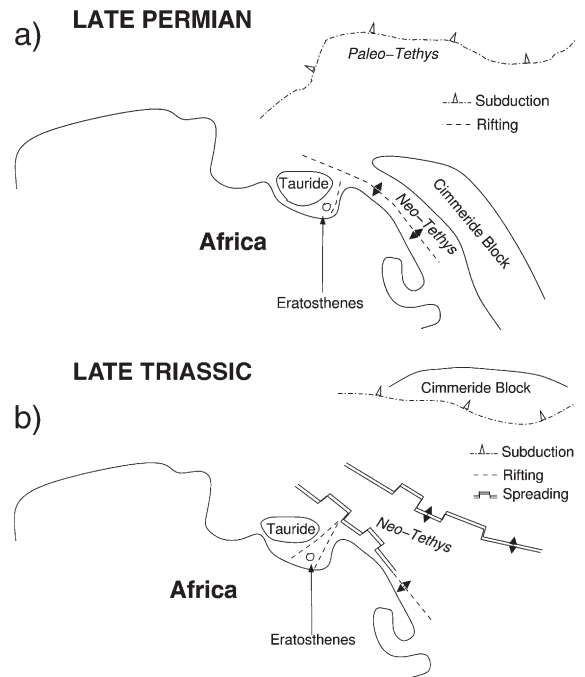

Fig. 18. (a) Reconstruction, modified after Garfunkel (1998). In the onset of the opening of the Neo-Tethys, many rifting axes existed, and an extensional regime moved the Eratosthenes Seamount northwest. (b) Continuation of the reconstruction into the Trias, likewise modified after Garfunkel (1998). The rifting axis south of the Cimmeride block has become a spreading axis, and Garfunkel also postulates a second spreading axis further north. The rift southeast of the Eratosthenes is still active, but does not reach the stage of seafloor spreading. The crust is significantly thinned, but still continental.

crust is generated. The N–S rifting southeast of the Eratosthenes Seamount does not reach the stage of spreading, and the Levantine Basin develops as a continental basin above stretched continental crust.

According to Walley (1998), extensional faults in both trends, E–W and NNE–SSW, represent zones of weaknesses during the compressional Syrian Arc events from the Late Cretaceous to the Early Miocene and develop into fold chains. We find only weak evidence of the NNE–SSW-trending Pelusium and Damietta–Latakia Lines. Where these lines cross our profiles, a little crustal thickening is observed.

8. Conclusions

Velocity distribution and structure of the crust along both profiles neither exhibit typical features of oceanic nor of continental crust, but resemble thinned continental crust found in other parts of the Mediterranean Sea. Comparison with the results of the DESERT2000-group (Weber et al., 2004) shows similarities in both structure

and velocity distribution and confirms the hypothesis of continental crust in the Levantine Basin. The β-factor can only be estimated between 2.25 and 5, depending on the choice of initial crustal thickness between 18 km under Galilee or 40 km under Jordan, but an assumption of 24 km yielding a β-factor of 3 seems reasonable. Comparison of the models of P1 and P2 with models of known ocean–continent transition zones and a rifted continental margin that did not reach the stage of sea-floor spreading revealed more similarities with the merely rifted margin than with the ocean–continent transition, which further confirmed our postulate of continental crust in the Levantine Basin.

Acknowledgements

References

Abdel Aal, A., El Barkooky, A., Gerrits, M., Meyer, H., Schwander, M., Zaki, H., 2000. Tectonic evolution of the Eastern Mediterraenan Basin and its significance for hydrocarbon prospectivity in the ultradeepwater of the Nile Delta. Lead. Edge 19, 1086–1102.

Albarello, D., Mantovani, E., Babbucci, D., Tamburelli, C., 1995. Africa–Eurasia kinematics: main constraints and uncertainties. Tectonophysics 243, 25–36.

Almagor, G., 1993. Continental slope processes off northern Israel and southernmost Lebanon and their relation to onshore tectonics. Mar. Geol. 112, 151–169.

Ben-Avraham, Z., Ginzburg, A., 1986. Magnetic anomalies over the central Levant continental margin. Mar. Pet. Geol. 3, 220–233.

Ben-Avraham, Z., Ginzburg, und, 1990. Displaced terranes and crustal evolution of the Levant and the eastern Mediterranean. Tectonics 9, 613–622.

Ben-Avraham, Z., Ginzburg, A., Makris, J., Eppelbaum, L., 2002. Crustal structure of the Levant Basin, eastern Mediterranean. Tectonophysics 346, 23–43.

Bohnhoff, M., Makris, J., Papanikolaou, D., Stavrakakis, G., 2001. Crustal investigation of the Hellenic subduction zone using wide aperture seismic data. Tectonophysics 343, 239–262.

Buck, W.R., 1991. Modes of continental lithospheric extension. J. Geophys. Res. 96, 20161–20178.

Dercourt, J., Zonenshain, L.P., Ricou, L.E., Kazmin, V.G., Le Pichon, X., Knipper, A.L., Grandjacquet, C., Sbortshikov, I.M., Geyssant, J., Lepverier, C., Boulin, D.V., Sibuet, J., Savostin, J. C., Sorokhtin, L.P., Westphal, D., Bazhenov, M., Laurer, M.L.,

Bijou-Duval, J.P., 1986. Geological evolution of the Tethys belt from the Atlantic to the Pamirs since the Lias. Tectonophysics 123, 241–315.

El-Isa, Z., Mechie, J., Prodehl, C., Makris, J., Rihm, R., 1987. A crustal structure study of Jordan derived from seismic refraction data. Tectonophysics 138, 235–253.

Farris, M.A., Griffiths, M.A., McGrandle, A., 2004. Deep structural lineaments: influence on basin evolution and cenozoic structuration in the East Mediterranean Levant Basin. PETEX 2004, London, 23–25 November 2004, London, Petroleum Exploration Society of Great Britain. extended abstracts on CDROM, unpaginated.

Freund, R., Goldberg, M., Weissbrod, T., Druckman, Y., Derin, B., 1975. The Triassic–Jurassic structure of Israel and its relation to the origin of the Eastern Mediterranean. Geol. Surv. Bull. (Israel) 65, 105–127.

Funck, T., Jackson, R., Louden, K.E., Dehler, S.A., Wu, Y., 2004. Crustal structure of the northern Nova Scotia rifted continental margin (eastern Canada). J. Geophys. 109. doi:10.1029/2004JB003008.

Gardosh, M., Druckmann, Y., in press. Stratigraphy and tectonic evolution of the Levantine Basin, offshore Israel. In: Robertson, A. (Ed), Tectonic Development of the Eastern Mediterranean Region, Geological Society Special Publication.

Garfunkel, Z., 1998. Constraints on the origin and history of the Eastern Mediterranean basin. Tectonophysics 298, 5–35.

Garfunkel, Z., 2004. Origin of the Eastern Mediterranean basin: a reevaluation. Tectonophysics 391, 11–34.

Ginzburg, A., Ben-Avraham, Z., 1987. The deep structure of the central and southern Levant continental margin. Ann. Tecton. 1, 105–115.

Ginzburg, A., Makris, J., Fuchs, K., Prodehl, C., Kaminski, W., Amiti, U., 1979. Seismic study of the crust and upper mantle of the Jordan–Dead Sea Rift and their transition toward the eastern Mediterranean. J. Geophys. Res. 84, 5605–5612.

Ginzburg, A., Ben-Avraham, Z., Makris, J., Hubral, P., Rotstein, Y., 1994. Crustal structure in northern Israel. Mar. Pet. Geol. 11, 501–506.

Gradmann, S., Hübscher, C., Ben-Avraham, Z., Gajewski, D., Netzeband, G.L., 2005. Salt tectonics off northern Israel. Mar. Pet. Geol. 22 (5), 597–611.

Hauser, F., O'Reilly, B.M., Jacob, A.W.B., Shannon, P.M., Makris, J., Voigt, U., 1995. The crustal structure of the Rockall Trough: differential stretching without underplating. J. Geophys. Res. 100, 4097–4116.

Hirsch, F., 1984. The Arabian sub-plate during the Mesozoic. In: Dixon, J.E., Robertson, A.H.F. (Eds.), Geological Evolution of the Eastern MediterraneanGeol. Soc. Spec. Publ. London, vol. 17, pp. 217–224.

Hirsch, F., Flexer, A., Rosenfeld, A., Yellin-Dror, A., 1995. Palinspastic and crustal setting of the eastern Mediterranean. J. Pet. Geol. 18, 149–170.

Hsü, K.J., Cita, M.B., Ryan, W.B.F., 1973. The origin of the Mediterranean Evaporites. In: Ryan, W.B.F., Hsü, K.J. (Eds.), Init. Repts. DSDP, vol. 13. U.S. Govt. Printing Office, Washington D.C., pp. 1203–1232.

Hsü, K.J., Monadert, L., Bernoulli, D., Cita, B.C., Erickson, A., Garrison, R.E., et al., 1978. History of the Mediterranean Salinity Crisis. In: Hsü, K.J., Montadert, L. (Eds.), Init. Repts. DSDP, vol. 42 I. U.S. Govt. Printing Office, Washington D.C., pp. 1053–1078.

Jiménez-Munt, I., Sabadini, R., Gardi, A., Bianco, G., 2003. Active deformation in the Mediterranean from Gibraltar to Anatolia

inferred from numerical modeling and geodetic and seismological data. J. Geophys. Res. 108, 2006. doi:10.1029/2001JB001544.

Kempler, D., Garfunkel, Z., 1994. Structures and kinematics in the northeastern Mediterranean: a study of an unusual plate boundary. Tectonophysics 234, 19–32.

Makris, J., Stobbe, C., 1984. Physical properties and state of the crust and upper mantle of the Eastern Mediterranean Sea deduced from geophysical data. Mar. Geol. 55, 347–363.

Makris, J., Ben-Avraham, Z., Behle, A., Ginzburg, A., Giese, P., Steinmetz, L., et al., 1983. Seismic reflection profiles between Cyprus and Israel and their interpretation. Geophys. J. R. Astron. Soc. 75, 575–591.

Makris, J., Papoulia, J., Papanikolaou, D., Stavrakakis, G., 2001. Thinned continental crust below northern Evoikos Gulf, central Greece, detected from deep seismic soundings. Tectonophysics 341, 225–236.

Mart, Y., 1982. Quaternary tectonic patterns along the continental margin of the southeastern Mediterranean. Mar. Geol. 327–344.

Mart, Y., 1984. The tectonic regime of the southeastern Mediterranean continental margin. Mar. Geol. 55, 365–386.

Mart, Y., Ben-Gai, Y., 1982. Some depositional patterns at the continental margin of the Southeastern Mediterranean Sea. AAPG Bull. 66, 460–470.

Mascle, J., Benkhelil, J., Bellaiche, G., Zitter, T., Woodside, J., Loncke, L., PRISMED II Scientific Party, 2000. Marine geologic evidence for a Levantine–Sinai plate, a new piece of the Mediterranean puzzle. Geology 28, 779–782.

Nafe, J., Drake, C., 1963. Physical properties of marine sediments. In: Hill, M.N. (Ed.), The Sea, vol. 3. Wiley, New York, pp. 794–815.

Neev, D., 1975. Tectonic evolution of the Middle East and the Levantine Basin (easternmost Mediterranean). Geology 3, 683–686.

Neev, D., 1977. The Pelusium Line—a major transcontinental shear. Tectonophysics 38, T1–T8.

Neev, D., Almagor, G., Arad, A., Ginzburg, A., Hall, J.K., 1976. The geology of the Southeastern Mediterranean Sea. Geol. Surv. Bull. (Israel) 68, 1–51.

Pätzold, J., Bohrmann, G., Hübscher, C., 2003. Black Sea–Mediterranean–Red Sea. METEOR-Berichte 03-2, Leitstelle METEOR. .

Peirce, C., Barton, P.J., 1992. Southern segment of the European Geotraverse—a wide-angle seismic refraction experiment in the Sardinia Channel. Mar. Geophys. Res. 14, 227–248.

Pérez-Gussinyé, M., Ranero, C.R., Reston, T.J., Sawyer, D., 2003. Mechanisms of extension at nonvolcanic margins: evidence from the Galicia interior basin, west of Iberia. J. Geophys. Res. 108, 2245. doi:10.1029/2001JB000901.

Pollack, H.N., Hurter, S.J., Johnson, J.R., 1993. Heat flow from the Earth's interior: analysis of the global data set. Rev. Geophys. 31, 267–280.

Robertson, A.H.F., 1998a. Mesozoic–Tertiary tectonic evolution of the easternmost Mediterranean area: Integration of marine and land evidence. In: Robertson, A.H.F., Emeis, K.-C., Richter, C., Camerlenghi, A. (Eds.), Proceedings of ODP, Science Results, vol. 160. Ocean Drilling Program, College Station, TX, pp. 723–782.

Robertson, A.H.F., 1998b. Tectonic significance of the Eratosthenes Seamount: a continental fragment in the process of collision with a subduction zone in the eastern Mediterranean (Ocean Drilling Program Leg 160). Tectonophysics 298, 63–82.

Robertson, A.H.F., Dixon, J.E., 1984. Introduction: aspects of the geological evolution of the Eastern Mediterranean. In: Dixon, J.E., Robertson, A.H.F. (Eds.), Geological Evolution of the Eastern Mediterranean. Geol. Soc. Spec. Publ. London, vol. 17, pp. 1–74.

Ryan, B.W.F., Stanley, D.J., Hersey, J.B., Fahlquist, D.A., Allan, T.D., 1970. The tectonics of the Mediterranean Sea. In: Maxwell, A.E. (Ed.), The Sea, vol. 4 II. Wiley, New York, pp. 387–491.

Sandwell, D.T., Smith, W.H.F., 1997. Marine gravity anomaly from Geosat and ERS 1 satellite altimetry. J. Geophys. Res. 102, 10039–10054.

Stampfli, G.M., Borel, G.D., 2002. A plate tectonic model for the Paleozoic and Mesozoic constrained by dynamic plate boundaries and restored synthetic ocean isochrons. Earth Planet. Sci. Lett. 196, 17–33.

Talwani, M., Worzel, L., Landisman, M., 1959. Rapid gravity computation for two dimensional bodies with application to the Mendocino submarine fracture zone. J. Geophys. Res. 64, 49–59.

Tibor, G., Ben-Avraham, Z., Steckler, M., Fligelmann, H., 1992. Late tertiary subsidence history of the southern Levant Margin, Eastern Mediterranean Sea, and its implications to the understanding of the Messinian Event. J. Geophys. Res. 97, 17593–17614.

Vidal, N., Alvarez-Marrón, J., Klaeschen, D., 2000a. Internal configuration of the Levantine Basin from seismic reflection data (Eastern Mediterranean). Earth Planet. Sci. Lett. 180, 77–89.

Vidal, N., Klaeschen, D., Kopf, A., Docherty, C., Von Huene, R., Krasheninnikov, V.A., 2000b. Seismic images at the convergence zone from south of Cyprus to the Syrian coast, eastern Mediterranean. Tectonophysics 329, 157–170.

Vogt, U., Makris, J., O'Reilly, B.M., Hauser, F., Readman, P.W., Jacob, A.W.B., Shannon, P.M., 1998. The Hatton Basin and continental margin: crustal structure from wide-angle seismic and gravity data. J. Geophys. Res. 103 (B6), 12545–12566.

Walley, C.D., 1998. Some outstanding issues in the geology of Lebanon and their importance in the tectonic evolution of the Levantine region. Tectonophysics 298, 37–62.

Weber, M., Abu-Ayyash, K., Abueladas, A., Agnon, A., Al-Amoush, H., Babeyko, A., Bartov, Y., Baumann, M., Ben-Avraham, Z., Bock, G., Bribach, J., El-Kelani, R., Förster, A., Förster, H.-J., Frieslander, U., Garfunkel, Z., Grunewald, S., Götze, H.J., Haak, V., Haberland, Ch., Hassouneh, M., Helwig, S., Hofstetter, A., Jäckel, K.-H., Kesten, D., Kind, R., Maercklin, N., Mechie, J., Mohsen, A., Neubauer, F.M., Oberhänsli, R., Qabbani, I., Ritter, O., Rümpker, G., Rybakov, M., Ryberg, T., Scherbaum, F., Schmidt, J., Schulze, A., Sobolev, S., Stiller, M., Thoss, H., Weckmann, U., Wylegalla, K., 2004. The crustal structure of the Dead Sea Transform. Geophys. J. Int. 156, 655–681.

Wessel, P., Smith, W., 1998. New, improved version of Generic Mapping Tools released. EOS, Trans. Am. Geophys. Union 79 (47), 579.

Woodside, J.M., 1977. Tectonics elements and crust of the Eastern Mediterranean Seamount. Mar. Geophys. Res. 3, 317–354.

Zelt, C.A., 1999. Modelling strategies and model assessment for wide-angle seismic traveltime data. Geophys. J. Int. 139, 183–204.

Zelt, C.A., Smith, R.B., 1992. Seismic traveltime inversion for 2-D crustal velocity structure. Geophys. J. Int. 108, 16–34.